A THIRTY CHANNEL REAL TIME AUDIO ANALYZER AND ITS APPLICATIONS

A THESIS

Presented to

The Faculty of the Division of Graduate Studies and Research

By

Joel Thomas Kalb

In Partial Fulfillment

of the Requirements for the Degree

Doctor of Philosophy in the School of Physics

Georgia Institute of Technology

February, 1975

A THIRTY CHANNEL REAL TIME AUDIO ANALYZER AND ITS APPLICATIONS

Approved:

Eugene T. Patronis, Jr., Chairman

J. Q. Williams

M. C. Payne, Jr.

Date approved by Chairman: 17 Feb. 75

ACKNOWLEDGMENTS

Sincere appreciation is extended to my advisor, Dr. Eugene T. Patronis, Jr., for the motivation and guidance which he provided me during this research. Further acknowledgment is extended to Drs. J. Q. Williams, M. C. Payne, Jr., and M. B. Sledd for their helpful comments.

The research reported herein was sponsored, in part, by an Industrial Fellowship from Schlumberger. I gratefully acknowledge this support.

I wish to give special thanks to Mrs. Carolyn Piersma for her work on this manuscript.

Finally, I am indebted to my parents, Mr. and Mrs. Henry T. Kalb, for their continued support and faith during my years of graduate study.

TABLE OF CONTENTS

LIST OF TABLES

LIST OF ILLUSTRATIONS

Figure Page

SUMMARY

Sound pressure levels in enclosed spaces are measured in a variety of ways. One which is particularly useful is a spectrum analysis in real time. Here a set of contiguous bandpass filters separate the signal into a collection of frequency bands. Then a corresponding set of detectors convert these bands to fluctuating rms equivalent values. Finally a multiplexer samples these quantities for a logarithmic display of the sequential band averages. This prompt and continuous representative spectrum allows effective analysis and modification of the properties of acoustic systems.

The purpose of this research is to interpret the spectrum average value in terms of the characteristics of realizable electrical networks and to employ recently developed integrated circuitry to construct an analyzer having optimum performance. Calculations were done for the power flow of a constant spectral slope noise signal through bandpass filters which are either ideal or of the Butterworth type. Then a comparison was made of the statistical properties of this narrow band signal after rectification by linear absolute value and square law detectors. Finally filter and detector designs were surveyed to obtain simple basic circuits which were accurate, stable and easily adjusted.

The conclusions reached are:

1. A Butterworth filter with three sections gives selectivity adequate for one third octave analysis of noise spectrums with slopes between -21 and +15 dB/octave.

2. For general broad band noise sources the linear absolute value detector performs as well as the preferred square law detector in view of the uncertainty of the averaged rms values.

3. A novel equalizer for spectrum modification can be constructed by using controlled amounts of filtered signals to interfere destructively with the original unfiltered signal.

CHAPTER I

INTRODUCTION

The Problem

In the study of acoustics, the most commonly measured quantity is the sound pressure level or SPL* as a function of either time or frequency. The sound pressure level meter gives the short term average value of the SPL as an indication of the sound pressure and consequent loudness as perceived by a listener. Further refinement using an oscilloscope to give the instantaneous value of the SPL against a time scale allows the determination of the transient or reverberant behavior of an acoustic system. Likewise, a real time spectrum analyzer consisting of a contiguous set of one third octave bandpass filters together with their associated detectors is able to average the sound pressure for the frequency components present in each band as an indication of the tonal quality of the sound. Additional high resolution frequency analysis with a 1 percent constant percentage bandwidth wave analyzer or a digital Fourier transform processor reveals the modes of resonance or harmonic generation in an acoustic system.

Just as a sound level meter with an averaging time of a few seconds gives a real time reading which may be used in making a control decision, the real time spectrum analyzer gives spectrum averages soon enough to determine a cause-effect relationship which is very useful in

---

*The definitions used in this work are discussed in Appendix B.

the adjustment of the frequency response of a given system. With this instrument large amounts of information may be quickly processed in order to give useful results for many sound control problems.

Real time analyzers consist of three principal parts--namely frequency selective networks, signal detection systems and a display device. The first such spectrum analyzers were constructed in 1939 by Freystedt [1], and in 1942 by Roop and Cook [2]. Each consisted of a set of 25 bandpass filters whose rectified outputs were averaged on storage capacitors. A mechanical multiplexer then sampled these averaged outputs thereby displaying on an oscilloscope a sequence of vertical bars, the heights of which were related to the rms value of the signal in each filter band. A logarithmic converter was included to give a vertical scale calibrated in decibels.

More recent real time analyzers [3,4] have extended dynamic signal range and improved selectivity as the result of the use of newer filter and detector designs. Also the use of transistorized circuits allow considerable savings in weight and electrical power. However, these analyzers tend to be prohibitively expensive since they include thirty multisection bandpass filters along with a matching set of detectors and storage elements, or else a single multiplexed analog to digital converter followed by an rms processor and magnetic core memory.

At present, the availability of integrated circuits allows the design and construction of economical real time analyzers having even better operational characteristics as compared with earlier passive network designs. One circuit of particular importance is the operational amplifier, a device once used mostly in analog computers, which

greatly simplifies the design of stable filters and detectors that are less complex, more accurate and easier to adjust. Another integrated circuit incorporates the excellent switching properties and small size of MOS field effect transistors making possible a compact inexpensive multiplexer.

Background to the Present Investigation

The present investigation leading to the construction of a real time analyzer centers on the characteristics of the signal filtering and detection networks. For the filters, the stagger tuned maximally flat or Butterworth design given in 1944 by Wallman [5] is outlined. The noise power transmitted by these filters when compared with ideal vertical sided filters gives a bandwidth related power error. This problem was studied in 1962 by Sepmeyer [6] in an effort to determine corrections giving an effective power bandwidth which would minimize this power error. Initially, Sepmeyer used a simplified straight sided filter model and determined:

(1) that the power error increases very rapidly for large values of spectrum slope;

(2) that the power error is symmetrical about a minimum value given by pink noise and that an optimum attenuation at the filter band edges exists for minimizing power errors as a function of spectrum slope.

Later [7] Sepmeyer revised his work by using the polynomial response function which describes the attenuation of Butterworth filters having two, three and four resonant stages; for octave, one half octave and one third octave bandwidths; and for noise slopes ranging from -12 to +6 dB/octave. These results were obtained by numerical integration

and have been adopted into the American Standard specification for filter sets [8]. Disadvantages of these results are that they are limited to just three filter bandwidths and that they deal with the attenuation at the nominal band edges, which is not as useful for design purposes as is the half power bandwidth. In this research, an analytic solution for the power transmitted by a general Butterworth filter with input noise spectrum slopes equal to integer multiples of 3 dB/octave leads to a knowledge of effective bandwidths and power errors for filters with any number of sections.

For audio frequency applications, the active bandpass filter most commonly utilized has been the twin T inverse feedback amplifier. This tuned amplifier is analyzed by Hastings [9] and shown to be stable over a wide range of amplifier conditions. The chief disadvantages of the circuit are that it requires close component matching and lacks a simple tuning mechanism. A more recent RC active design [10] employing multiple inverse feedback around an operational amplifier is easily adjusted for both gain and bandwidth. Other advantages of this filter are that it requires only 5 to 10% tolerance components and is relatively insensitive to component changes with time and temperature. Its chief shortcoming is a tendency to become unstable and inaccurate for frequencies above 1 kHz where the amplifier often has reduced gain and increasing phase lag. These limitations are investigated in order to establish the range of applicability of the circuit. A modified Wien Bridge [11] filter which is used for higher frequencies will also be discussed.

After the noise signal is filtered, its rms value is measured by a nonlinear device called a detector. The value measured depends on the

statistical properties of the noise signal. This was considered for many common situations in a classic paper by Rice in 1944 [12]. These results were later applied to random noise in narrow band filters for vibration analysis by Morrow in 1958 [13]. In the present work, these results are extended to the case of the absolute value linear detector which may be accurately constructed with an operational amplifier along with feedback silicon diodes. This detector is compared to the square law detector used in previous analyzers. In each case, the average detector output and low frequency fluctuations are calculated for broad band random noise signals encountered in steady acoustic signals.

Use of One Third Octave Bandwidths

The use of one third octave filter bandwidths in spectrum analysis is based on the frequency selective behavior of the ear. In 1953 Fletcher [14] showed that the hearing process involves a critical bandwidth within which the sensation of loudness is due to the strongest frequency component. Later using perceived loudness as an indication, Zwicker [15] measured these critical bands by varying the bandwidth of random noise while maintaining a constant sound pressure level. For wide band noise, the loudness was proportional to the bandwidth, but when the noice was included within a critical band the loudness remained constant. These critical bandwidths were found to be close to one third octaves for frequencies between 280 Hz and 14 kHz. Below 280 Hz the bandwidths increased to one octave at the lowest audible frequencies. For loudness studies, these results indicate that it is sufficient to resolve the spectrum into one third octave bands since the loudness measurement is independent of the spectral distributions within these bands.

Equalization of Electro-acoustical Systems

Equalization networks have long been used in compensating for frequency response deficiencies and noise generation in devices such as audio amplifiers, phonograph recordings and magnetic tape recorders. Since their transfer responses and noise power vary gradually with frequency, the required correction circuits were simple and inexpensive. Only recently have these same methods been applied to electro-acoustical systems used to reinforce the sound level in enclosed spaces. In these electro-acoustical systems, the electrical part consists of microphones, amplifiers and loudspeakers, while the room surfaces and volume determine the acoustic portion.

If a microphone is included in this system, possible instability or howlback may occur if the sound pressure fed back from the loudspeakers is in phase and greater in amplitude than the original input sound. This instability is studied by Schroeder [16], Bonner and Bonner [17] and Waterhouse [18]. Treatment is difficult since several components of the system influence the transmission of the sound. If the resonances in the electrical system are minimized and the direct feedback is reduced by the use of directional microphones and loudspeakers which are properly placed, the problem remains as a result of reverberant sound reflected from the room walls and other surfaces. Schroeder has shown that the sound spectrum in a large room varies over a 30 dB range with peaks separated by an average of 20 Hz. These response peaks or room modes overlap and are capable of modifying the amount of sound energy which reaches the microphone.

This problem can be treated with active filters similar to those

which are utilized in the analyzer. The signal energy transmitted through octave or one third octave bands is adjusted to minimize the system resonances. Next the amplifier gain is increased until howl-back occurs. Finally these oscillations are removed with adjustable narrow band filters. The one third octave real time analyzer is essential in this operation since it continuously displays the spectrum showing the interactions of the equalization adjustments. This allows for optimum equalization of the room for either music or speech and for subsequent modifications based on changes in the room environment caused by the absorption of sound by an audience and by the alteration of propagation velocity with changes in air temperature.

CHAPTER II

THEORETICAL CONSIDERATIONS

Bandpass Filter Characteristics

The sound pressure level spectrum of a given noise signal will be estimated by separating the frequency components with narrow band filters tuned to standard one third octave frequencies. The average signal which each filter transmits depends on the filter bandwidth and degree of complexity along with the spectral slope of the noise. A preliminary description of these influences as well as a standard for reference will be obtained by considering the filter to be ideal; that is, the filter passes uniformly those signal components within its passband while rejecting all others. Similar analysis of the maximally flat Butterworth filter leads to preferred values of filter bandwidth and complexity for given center frequencies and noise slopes.

The quantity which will represent the signal in these calculations is the power spectral density W(f). The average power dissipated in a resistance of one ohm by those signal components having frequencies whose absolute values lie between f and f + df is W(f)df. For the present discussion, all the power will be associated with only positive frequencies thus giving a one-sided power spectrum. If the microphone voltage is assumed proportional to the sound pressure, the power spectrum will vary as the square of the sound pressure spectrum. The principal reason for considering the power spectral density is that a simple relation [19] exists between the input and output spectrums of a linear

device which has system transfer function A(f), such that

$$W_{out}(f) = |A(f)|^2 W_{in}(f) \quad . \tag{1}$$

Hence, if the input spectrum is known to be simple such as for white noise with equal power per unit frequency or pink noise with equal power per unit octave, then measurement of the output spectrum yields information about the magnitude of the system response function. Many other noise sources are conveniently described by the spectral density functions

$$W_{in}(f) = W_o(f/f_o)^m \tag{2}$$

having slopes of m x 3 dB/octave when plotted on a logarithmic frequency scale. Typical room spectra have straight line slopes in several regions of the audio band. Common examples are listed in Table 1. In the course of preparing standards [20] for acoustic filter sets the specifications writing group examined thirty representative spectra of noise measurements made in the field and found noise slopes ranging from m values of -7 to +2.

The frequency response of the ideal one third octave bandpass filter is shown in Figure 1 along with the Butterworth filter responses of single and triple stages. The cutoff frequencies f_1 and f_2 correspond to the half-power frequencies of the Butterworth filters and to the band edges of the ideal filter. In the case of filters with bandwidth fraction R and band center frequency f_o, these 3 dB frequencies are related by

Table 1. Common Noise Spectral Slopes

Spectral Slope	Noise
m = 0	White noise or thermal noise
m = -1	Pink noise or 1/f noise
m = -2	RC lowpass filtered white noise beyond the cutoff frequency
m = -4	LC lowpass filtered white noise beyond the cutoff frequency
m = 4	White noise spectrum below first resonant frequency of infinite baffle direct radiator loudspeaker
m = 6	White noise spectrum below first resonant frequency of bass reflex loudspeaker

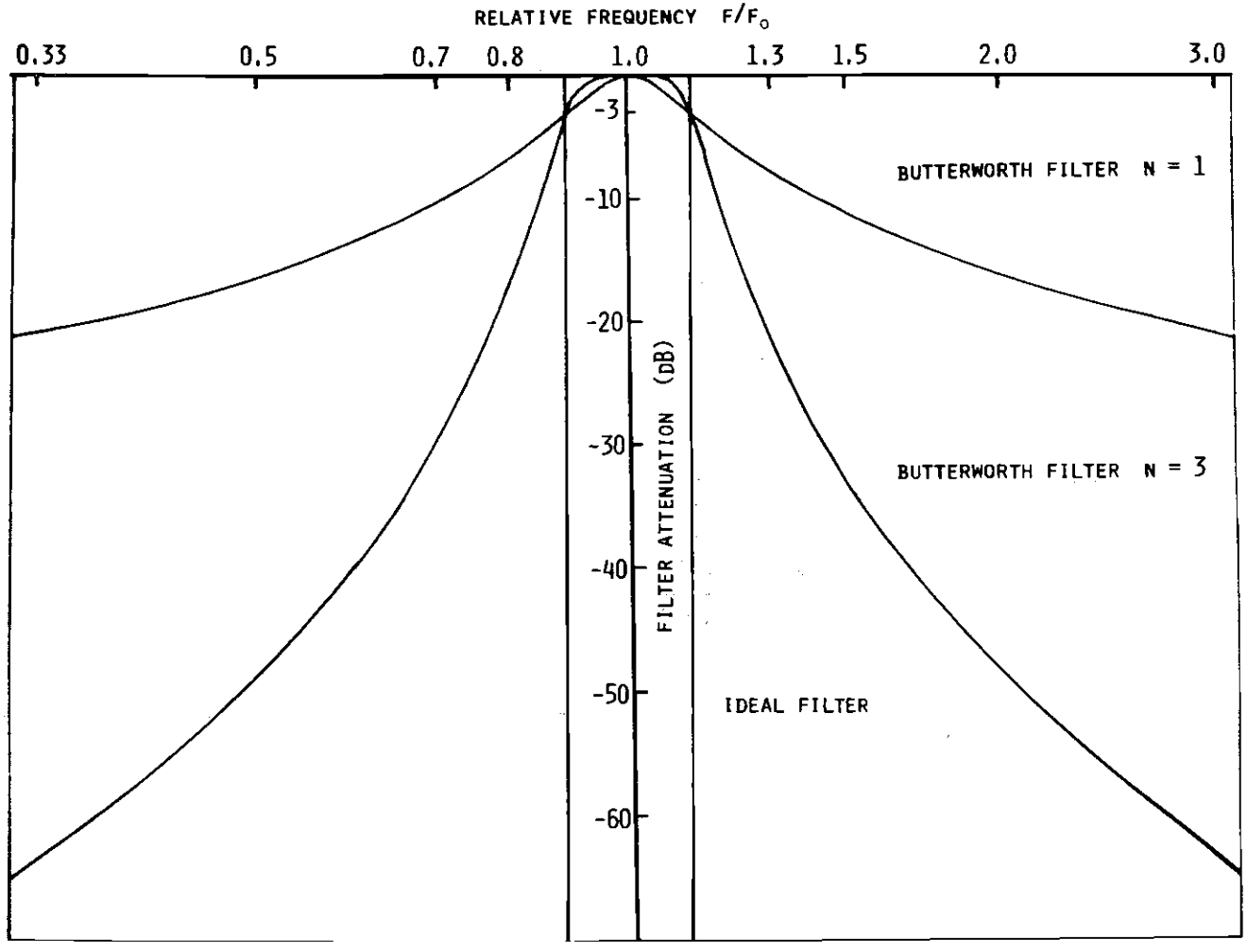

Figure 1. Frequency Response of Three Kinds of Bandpass Filters.

$$\frac{f_2}{f_1} = 2^R \ , \tag{3}$$

and

$$f_1 \ f_2 = f_o^{\ 2} \ , \tag{4}$$

leading to

$$f_1 = 2^{-R/2} \ f_o \ , \tag{5}$$

$$f_2 = 2^{+R/2} \ f_o \ . \tag{6}$$

The nominal bandwidth or half power bandwidth of the filters is

$$B = f_1 - f_2 = f_o(2^{R/2} - 2^{-R/2}) \ . \tag{7}$$

Two other dimensionless filter design quantities which may now be defined are the filter selectivity Q and the dissipation or damping factor δ, where

$$Q = \frac{1}{\delta} = f_o/B \ . \tag{8}$$

One important result which follows from the definition of the center frequency f_o in (4) is that the filter response is geometrically symmetric about that frequency. This means that the magnitude of the filter transfer function is the same for those pairs of frequencies f and $f_o^{\ 2}/f$ having f_o as their geometric mean value.

The total power passed by the ideal filter for noise slope m is found by integration.

$$P_I(m,R) = \int_0^{\infty} W_{out}(f)df = \int_{f_1}^{f_2} W_o f_o (f/f_o)^m df \tag{9}$$

$$= W_o f_o \, R \ln(2) \quad , \quad m = -1 \tag{10}$$

$$= W_o f_o \frac{1}{(m+1)} \left(2^{(m+1)R/2} - 2^{-(m+1)R/2} \right) \quad , \quad m \neq -1 \; . \tag{11}$$

The spectral slope dependence of this power is shown by the solid curve of Figure 2 for the case of a one third octave bandwidth, R = 1/3. As shown, the least power flows for pink noise input i and the power flow increases equally for slopes m and -(m + 2). As indicated in the General Radio Noise Handbook [21], this increased power flow occurs because the energy passed by the filter in the region where the signal level is high will more than counterbalance the decrease in energy in the opposite region. A similar effect results in filling in a narrow dip and rounding off the top of a peak in a spectrum. It is merely what is to be expected from the limitations in resolution of a finite bandwidth.

The Butterworth filter which is now studied readily approximates the ideal filter since it has the flattest bandpass response of any filter for a given number of stages. Outside the band the filter response approaches asymptotically a constant rolloff rate which increases by 6 db per octave for each stage of the network.

In 1930 Butterworth found that rapid rolloff frequency responses for low pass filters could be obtained by cascading frequency selective amplifiers [22]. In 1944 Wallman [23] extended Butterworth's work by stagger tuning single section bandpass amplifiers producing a relatively flat bandpass response along with a rapid initial rolloff at the band

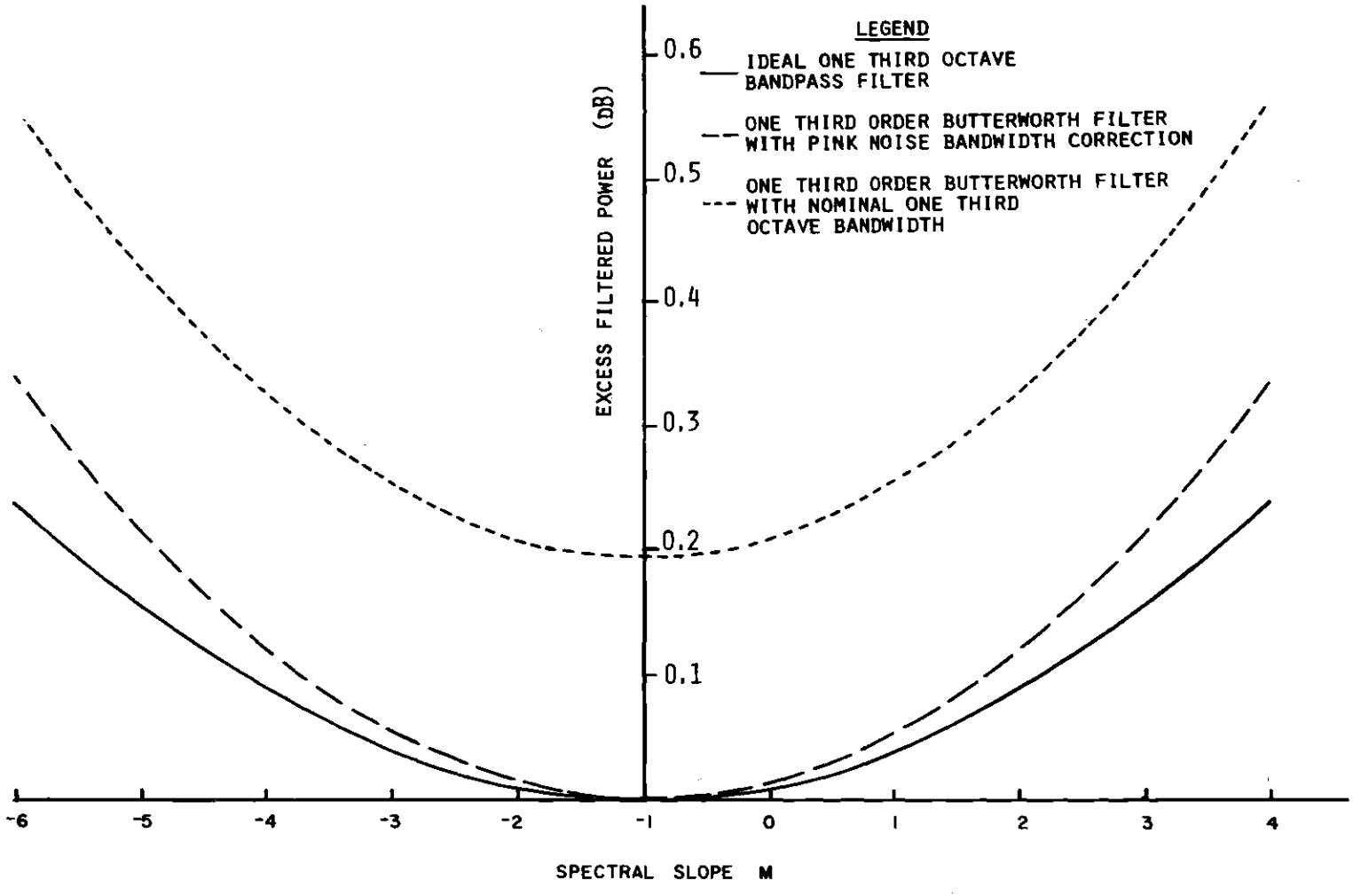

Figure 2. Filtered Noise Power in Excess of the Pink Noise Power Passed by the Ideal One Third Octave Filter.

edges. These circuits of Butterworth and Wallman offered simplicity in adjustment and design as a result of the buffering action of the amplifier in each stage. The isolation provided by these amplifiers allowed the straightforward synthesis of any complex transfer function which could be factored into simpler biquadratic terms.

As an example, the transfer function of the parallel RLC bandpass network with current source input I(s) and output voltage E(s) is given by

$$A(s) = \frac{E(s)}{I(s)} = \frac{A_o \, \delta(s/\omega_o)}{(s/\omega_o)^2 + \delta(s/\omega_o) + 1} \, . \tag{12}$$

In terms of the component values the resonant frequency, damping factor, and midband response are

$$\omega_o = 2\pi f_o = (LC)^{-\frac{1}{2}} \, , \tag{13}$$

$$\delta = R_o (L/C)^{\frac{1}{2}} \, , \tag{14}$$

$$A_o = A(i\omega_o) = R_o \, . \tag{15}$$

For a steady state input the magnitude of the response function is

$$/A(f)/ = \frac{A_o}{\left(1 + \left[\frac{1}{\delta}\left(\frac{f}{f_o} - \frac{f_o}{f}\right)\right]^2\right)^{\frac{1}{2}}} \tag{16}$$

and the band edge response is

$$|A(f_1)| = |A(f_2)| = A_o / \sqrt{2} \, . \tag{17}$$

The maximally flat response for a filter with unity midband gain has a similar form

$$/A(f)/ = \frac{1}{\left(1 + \left[\frac{1}{\delta}\left(\frac{f}{f_o} - \frac{f_o}{f}\right)\right]^{2n}\right)^{\frac{1}{2}}} , \tag{18}$$

where n is the order of complexity or number of stages in the filter. This transfer function of order n can be synthesized by combining n first-order bandpass filters arranged in pairs. The k-th pair has dissipation factors d_k and midband gain A_{o_k}, while the two center frequencies $f_o\,\alpha_k$ and f_o/α_k have f_o as their geometric mean. If n is odd, there is one additional filter centered on f_o with the same dissipation factor δ as for the compound filter and with unity midband gain. These factors for the dissipation, offset tuning and midband gain are,

$$d_k^{\,2} = \frac{4 + \delta^2 - \sqrt{16 + 8\delta^2 \cos\frac{(2k-1)\pi}{n} + \delta^4}}{2} , \tag{19}$$

$$a_k = \frac{1}{2}\sqrt{\delta^2 - d_k^{\,2}} + (\delta/d_k)\sin(2k-1)\pi/2n , \tag{20}$$

$$A_{o_k} = \delta/d_k , \tag{21}$$

where

$k = 1,2,\ldots,n/2$ n even ,

$k = 1,2,\ldots,(n-1)/2$ n odd .

Power Transmitted through Butterworth Filters

It is now possible to calculate the power transmitted through the

n-th order bandpass filter with noise input having a spectral density with slope m. Of particular interest is the excess power which is transmitted outside the nominal passband due to the finite attenuation of the filter. To obtain a measure of the resolution capability of the n-th order filter, its output spectrum will be integrated over a band of frequencies centered on f_o with octave bandwidth fraction r. This is given by,

$$P = P(m,n,\delta,r) = \int_{f-}^{f+} \frac{W_o (f/f_o)^m \, df}{1 + \left[\frac{1}{\delta}\left(\frac{f}{f_o} - \frac{f_o}{f}\right)\right]^{2n}} , \tag{22}$$

where from equations (5,6) with R replaced by r the border frequencies are

$$f- = 2^{-r/2} f_o , \tag{23}$$

$$f+ = 2^{+r/2} f_o . \tag{24}$$

Substituting a new frequency variable x, where

$$f/f_o = e^x , \tag{25}$$

gives

$$P = \int_{x-}^{x+} \frac{W_o f_o \, e^{(m+1)x} \, dx}{1 + \left[\frac{1}{\delta}\left(e^x - e^{-x}\right)\right]^{2n}} \tag{26}$$

where

$$x\pm = \pm(r/2) \ln(2) . \tag{27}$$

If the frequency x is replaced by -x and the resulting expression for P is averaged with equation (26), the result is

$$P = W_o f_o \, 2(\delta/2)^{2n} \int_0^{x+} \frac{\cosh\,(m+1)x\,dx}{(\delta/2)^{2n} + \sinh^{2n} x} \,. \tag{28}$$

This expression shows that the power has the same dependence on m as indicated in Figure 2 for the ideal filter,

$$P(m,n,\delta,r) = P(-(m+2),n,\delta,r) \,. \tag{29}$$

Also the requirement that the total power be finite leads to a restriction on the values of m,

$$-(2n+1) < m < 2n = 1 \,. \tag{30}$$

The procedure for evaluating the power in equation (28) begins by factoring the numerator into a cosh x term and a polynomial involving only even powers of sinh x. Next, the denominator is factored into n terms involving $\sinh^2 x$ and the n n-th roots of $-(\delta/2)^{2n}$. The resulting rational function in $\sinh^2 x$ is then expanded as a sum of partial fractions which may be integrated. The form of the integrals depends on the cosh x term which is present for even noise slopes and missing for odd slopes. Finally, the total power passed by the filter may be found by taking the limit of these expressions for large octave bandwidth fractions r. For even noise slopes, the total power can be found by direct integration of equation (28).

Following Gradshteyn and Rhyzik [24], Equations 1.30, 1.332-3, and 1.332-4, give the required expansions of cosh (m + 1)x which are

listed in Table 2. The general form of the expressions for the A coefficients is

$$A_{2k}(m) = \left(\frac{m+1}{2}\right) \frac{((m+2k-1)/2)!}{((m-2k+1)/2)!} \frac{2^{2k}}{(2k)!} \quad , \; m \geq 1 \text{ and odd} \tag{33}$$

$$= \frac{((m+2k)/2)!}{((m-2k)/2)!} \frac{2^{2k}}{(2k)!} \quad , \; m \geq 0 \text{ and even} \tag{34}$$

The denominator of equation (28) is an n-th order polynomial in the variable $\sinh^2 x$ and may be factored into n terms containing its roots $\chi_\ell^2(n)$,

$$\sinh^{2n} x + (\delta/2)^{2n} = \prod_{\ell=1}^{n/2} (\sinh^2 x - \chi_\ell^2(n))(\sinh^2 x - \chi_\ell^2(n)^*) \tag{35}$$

for n even, and

$$= \left[\prod_{\ell=1}^{(n-1)/2} (\sinh^2 x - \chi_\ell^2(n))(\sinh^2 x - \chi_\ell^2(n)^*)\right](\sinh^2 x - \chi^2_{\frac{n+1}{2}}(n))$$

for n odd, (36)

where the roots are

$$\chi_\ell^2(n) = (\delta/2)^2 \, e^{i(2\ell-1)\pi/n} \; . \tag{37}$$

In the expansion by partial fractions of the integrand in equation (28) there are four cases depending on whether m and n are even or odd. As an example in the case where m and n are both odd the integrand is,

Table 2. Expansion Coefficients of cosh (m + 1)x

Case I - m odd

$$\cosh (m+1)x = A_0 + A_2\sinh^2 x + \ldots + A_{2k}\sinh^{2k} x \ldots = A_{m+1}\sinh^{m+1} x \quad (31)$$

where the coefficients are

m	cosh (m + 1)x	A_0	A_2	A_4	A_6
-1	cosh 0x	1	0	0	0
1	cosh 2x	1	2	0	0
3	cosh 4x	1	8	8	0
5	cosh 6x	1	18	48	32

Case II - m even

$$\cosh (m+1)x = \cosh x\,(A_0 + \ldots + A_{2k}\sinh^{2k} x + \ldots + A_m\sinh^m x) \quad (32)$$

where

m	cosh (m + 1)x	A_0	A_2	A_4	A_6
0	cosh x	1	0	0	0
2	cosh 3x	1	4	0	0
4	cosh 5x	1	12	16	0
6	cosh 7x	1	24	80	64

$$\frac{(\delta/2)^{2n} \sum_{k=0}^{(m+1)/2} A_{2k} \sinh^{2k} x}{\sinh^{2n} x + (\delta/2)^{2n}} = \sum_{\ell=1}^{(n-1)/2} \left(\frac{B_\ell}{\sinh^2 x - \chi_\ell^2} + \frac{B_\ell^*}{\sinh^2 x - \chi_\ell^{2*}} \right)$$

$$+ \frac{B_{(n+1)/2}}{\sinh^2 x - \chi^2_{\frac{n+1}{2}}} \qquad (38)$$

The expansion coefficient B_ℓ may be evaluated by multiplying both sides of this equation by the associated denominator and letting $\sinh^2 x$ approach χ_ℓ^2. The expression on the left is indeterminate since both the numerator and denominator vanish when the limit is taken. However, application of L'Hospital's rule gives

$$B_\ell = -(1/n) \sum_{k=0}^{(m+1)/2} A_{2k}(m) \, (\chi_\ell^2)^{k+1} \qquad (39)$$

Integration of the partial fractions leads to integrals of two forms depending on whether m is odd or even. In these two cases, the integrals are

$$I_\ell(m,n,\delta,r) = 2 \int_0^{x+} \frac{dx}{\sinh^2 x - \chi_\ell^2} \quad m \text{ odd} , \qquad (40)$$

and

$$= 2 \int_0^{x+} \frac{\cosh x \, dx}{\sinh^2 x - \chi_\ell^2} \quad m \text{ even} . \qquad (41)$$

These integrals may be evaluated by elementary methods giving the results

listed below for finite and infinitely large bandwidth fractions r. For odd m,

$$I_\ell(m,n,\delta,r) = (2i/\eta)[\log(1 - \zeta - i\eta) - \log(1 - \zeta + i\eta) + \log(2^r - \zeta + i\eta) + \log(2^r - \zeta - i\eta)] , \quad (42)$$

and for $r \to \infty$

$$I_\ell(m,n,\delta,\infty) = (2i/\eta)[\log(1 - \zeta - i\eta) - \log(1 - \zeta + i\eta)] , \quad (43)$$

where

$$\eta = \sqrt{(1 - \zeta^2)} , \quad (44)$$

and

$$\zeta = 1 + 2\chi_\ell^2. \quad (45)$$

For even m,

$$I_\ell(m,n,\delta,r) = (1/\chi_\ell)[\log(\sinh x+ - \chi_\ell) - \log(\sinh x+ + \chi_\ell) + i\pi], \quad (46)$$

where x+ is given by equation (26).

For $r \to \infty$,

$$I_\ell(m,n,\delta,\infty) = i\pi/\chi_\ell. \quad (47)$$

Since both log z and $\sqrt{z}$ are multiple valued functions of the complex variable z, they must be made single valued functions in order to obtain a physically meaningful value for the output power. This is done by choosing the principal branch of log z for which

$$-\pi < \text{Arg } z \leq \pi \tag{48}$$

and by choosing that branch of $\sqrt{z}$ which gives positive real values for η in equation (44) for purely imaginary values of ζ.

Finally, by noting that the terms for B_ℓ and B_ℓ^* in equation (38) are complex conjugates, the results may be abbreviated for both odd and even values of m and n as

$$P(m,n,\delta,r) = W_o f_o \left\{ \sum_{\ell=0}^{(n-1)/2} 2\, \text{Re}\{B_\ell(m,n)\, I_\ell(m,n,\delta,r)\} + B_{(n+1)/2}\, I_{(n+1)/2} \right\} , \quad \text{for } n \text{ odd} \tag{49}$$

$$= W_o f_o \sum_{\ell=0}^{n/2} 2\, \text{Re}\{B_\ell(m,n)\, I_\ell(m,n,\delta,r)\} , \quad \text{for } n \text{ even} \tag{50}$$

where

$$B_\ell(m,n) = -(1/n) \sum_{k=0}^{(m+1)/2} A_{2k}(m)(\chi_\ell^2)^{k+1} , \quad \text{for } m \text{ odd} \tag{51}$$

$$= -(1/n) \sum_{k=0}^{m/2} A_{2k}(m)(\chi_\ell^2)^{k+1} , \quad \text{for } m \text{ even} . \tag{52}$$

In those cases where the noise power spectrum has even slope, the total output power for any n is found by integrating equation (28) directly with the substitution $u = (\delta/2) \sinh x$,

$$P(m,n,\delta,\infty) = W_o f_o \delta \sum_{k=0}^{m/2} A_{2k} (\delta/2)^{2k} \int_0^\infty \frac{u^{2k}\, du}{u^{2n} + 1} \tag{53}$$

$$= W_o f_o \delta \sum_{k=0}^{m/2} A_{2k} (\delta/2)^{2k} \left[\frac{\pi}{2n} \frac{1}{\sin (2k+1)\pi/2n}\right] . \tag{54}$$

This expression becomes particularly simple in the case of white noise,

$$P(0,n,\delta,\infty) = W_o f_o \delta \frac{\pi}{2n} \frac{1}{\sin \frac{\pi}{2n}} . \tag{55}$$

Power Errors and Bandwidth Correction Factors

Equation (55) may be compared to the result for the white noise transmitted by the ideal filter, by using equations (7, 8, 11)

$$P_I(0,R) = W_o f_o (2^{R/2} - 2^{-R/2}) = W_o f_o \delta = W_o B . \tag{56}$$

Thus for white noise, one finds the unique result that the power passed by either filter is proportional to the nominal bandwidth B. In addition, the realizable filter output power approaches the ideal filter power as the order of complexity n increases. This realizable power is in excess of the ideal value by a multiplicative factor called the power error H(m,n,R). For white noise this is,

$$H(0,n,R) = \frac{P(0,n,\delta,\infty)}{P_I(0,R)} = \frac{\pi}{2n} \frac{1}{\sin \frac{\pi}{2n}} . \tag{57}$$

Sepmeyer [25] corrects this factor to unity by reducing the damping factor δ in equation (55) to the new corrected value δ'. The ratio of

the nominal bandwidth B to the corrected bandwidth B' is called the bandwidth correction factor K(m,n,R) and is given by,

$$K(m,n,R) = \frac{B}{B'} = \frac{\delta}{\delta'} \quad . \tag{58}$$

In the special case of white noise,

$$K(0,n,R) = \frac{\pi}{2n} \frac{1}{\sin \frac{\pi}{2n}} = H(0,n,R) \tag{59}$$

where the equality is due to the linear relation between the filtered power and the filter bandwidth. Also, the correction factor does not depend on R so it is the same for all filter bandwidths.

Similar analysis using pink noise leads to the bandwidth correction factor K(-1,n,R). This involves using equations (10, 49, 50, 51) to equate the realizable and ideal filter outputs,

$$P(-1,n,\delta',\infty) = W_o f_o \; R \ln 2 \tag{60}$$

and solving for the corrected damping factor δ'. Since the expressions for the realizable power are not simply related to the octave bandwidth fraction R, the modified damping factor is found by calculation of the power for different values of δ' until equation (60) is satisfied. The results of the bandwidth correction factors for both pink and white noise are listed in Table 3 for filters up to the fourth order and for octave, one half octave and one third octave bandwidths. For the pink noise case, the correction factor is no longer independent of the bandwidth since the correction decreases with increasing values of R and n. For practical tuning either noise correction is the same for filters above

Table 3. Bandwidth Correction Factors Versus Bandwidth for Pink and White Noise Input

n	Octave (R = 1)	One Half Octave (R = 1/2)	One Third Octave (R = 1/3)
	Pink Noise K(-1,n,R)		
1	1.384987	1.469649	1.501399
2	1.092409	1.104789	1.107827
3	1.040835	1.045386	1.046367
4	1.022920	1.025280	1.025768
	White Noise K(0,n,R)		
1	1.570796	1.570796	1.570796
2	1.110721	1.110721	1.110721
3	1.047198	1.047198	1.047198
4	1.026172	1.026172	1.026172

second order and for bandwidths of one third octave or less. Significant differences appear for the wider bandwidths, particularly in the first order filter.

The power from both the pink noise corrected and nominal one third octave filter is plotted versus noise slope in Figure 2. The effect of the correction is to reduce the worst case power excess to less than 0.3 dB and to within 0.1 dB of the ideal filter response.

Resolution of the Power Spectrum

In Figure 3, the power $P(m,n,\delta,r)$ is shown as a percentage of the total output power $P(m,n,\delta,\infty)$ for different filter orders and for a range of input spectral slopes. Also shown for reference is the pink noise response of the ideal filter. Here 100% of the energy flows within the nominal one third octave bandwidth. In the case of the three section filter, this figure is 88.3%, and for the single section filter, 65%. The departure from the ideal filter resolution can be measured by considering the bandwidth which encloses 95% of the power. For the third order filter, this bandwidth is approximately one half octave wide extending one quarter of the way into each adjacent one third octave band, while for the first order filter, the corresponding bandwidth of 5/3 octave contains two bands on either side of the center band. Also shown for comparison is the commonly used single section filter with uncorrected, nominal one third octave bandwidth. While the pink noise power extends over the same width as the corrected single section filter, the percentage within the nominal band is reduced to 53%. For the worst case noise slopes, the response increasingly deviates from the ideal for fewer numbers of stages due to the inadequate attenuation at the filter skirts.

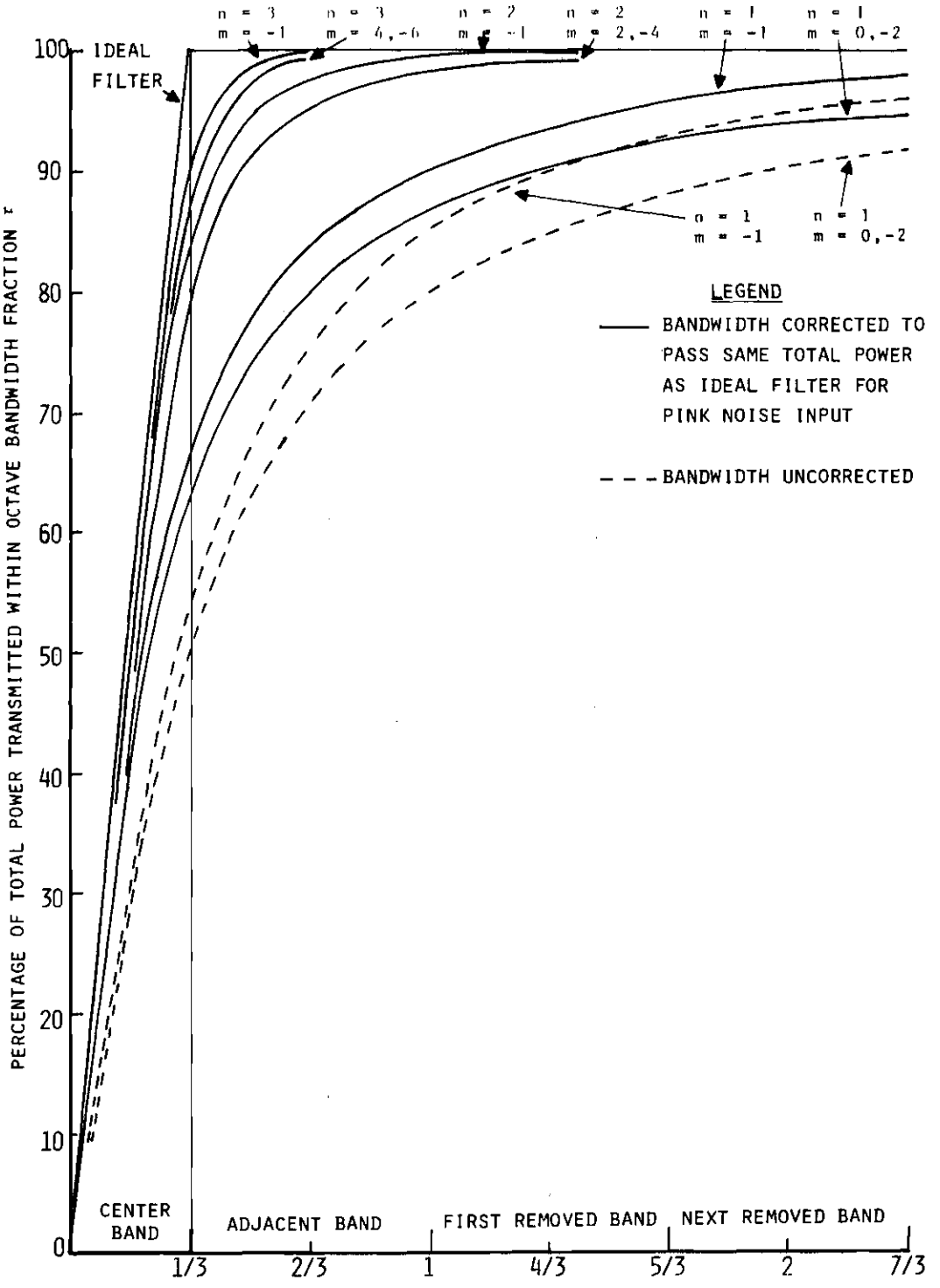

Figure 3. Fractional Power Transmitted in Octave Bandwidth Fraction r.

In conclusion, the one third octave filter is seen to resolve the power adequately while not being excessively complex. The pink noise corrections and white noise bandwidth correction factors can be used interchangeably in most situations. Finally, the power error for the corrected one third octave filter differs negligibly from that for the ideal filter over the range of allowable input noise slopes.

RC Active Filters

RC active filters may be used to construct a cascade network which has the Butterworth frequency response as indicated by equation (18). These filters offer several advantages over the passive RLC network to synthesize the general bandpass transfer function of equation (12). Several active filter design approaches exist which differ both in the choice of an active element and in the application of the feedback necessary to produce the complex conjugate pole pairs of A(s). Important considerations in the choice of a design are the ease of adjustment, number of components, degree of sensitivity to component value changes, and conditions for stability.

The main problem with the RLC network lies in the inductor L which is large and not easily adjusted for the lower audio frequencies. Also, since there is no buffering element, the cascaded stages interact making design and adjustment difficult. The RC active filter overcomes these faults but brings with it the new problems of noise and the possibility of oscillations.

The multiple feedback design of Holt and Sewell [26] employs an operational amplifier connected in the inverting mode as shown in Figure 4. Since proper operation of this filter depends on the

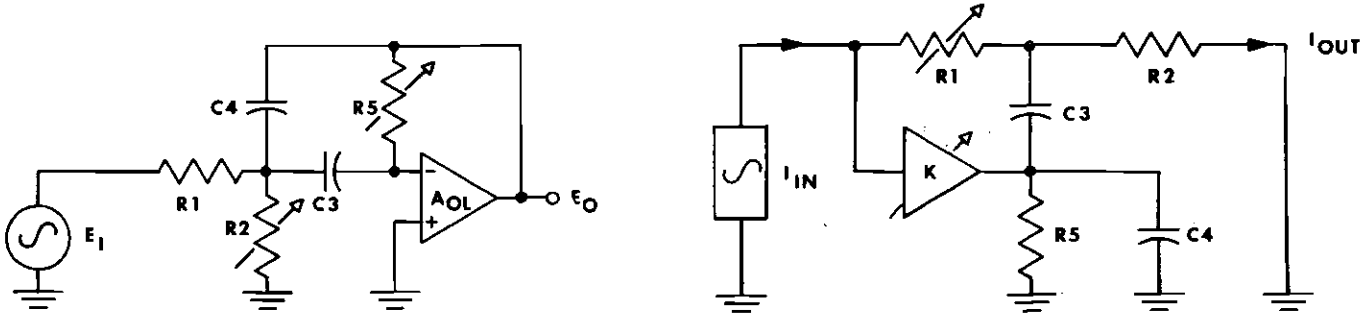

Figure 4. Active Filter Networks Used in the Construction of the Analyzer.

maintenance of at least 60 dB of open loop gain over the frequency range of interest, the 741 operational amplifier which was available at the start of the present work could not be used over the entire audio range. For frequencies beyond 1 kHz a filter consisting of a Wien bridge connected to give positive feedback around a fixed gain dual transistor current amplifier was employed. Recently developed feedforward compensation techniques [27] when applied to the LM101A operational amplifier would allow coverage of the entire audio range with filters of the multiple inverse feedback type. By following the analysis of the multiple feedback filter of Figure 5 given by Heulsman [28], the general transfer function

$$A(s) = \frac{-Y_1 Y_3}{[(Y_1+Y_2+Y_3+Y_4)Y_5+Y_3Y_4]+\frac{1}{A_{OL}}[(Y_1+Y_2+Y_3+Y_4)(Y_5+Y_6)+Y_3(Y_1+Y_2+Y_4)]} \tag{61}$$

is given terms of the admittances

$$\begin{aligned} Y_1 &= 1/R_1 \\ Y_2 &= 1/R_2 \\ Y_3 &= s\ C_1 \\ Y_4 &= s\ C_2 \\ Y_5 &= 1/R_5 \\ Y_6 &= 1/R_{IN} \end{aligned} \tag{62}$$

Here R_{in} represents the input impedance of the operational amplifier which is 2 Megohms for the 741.

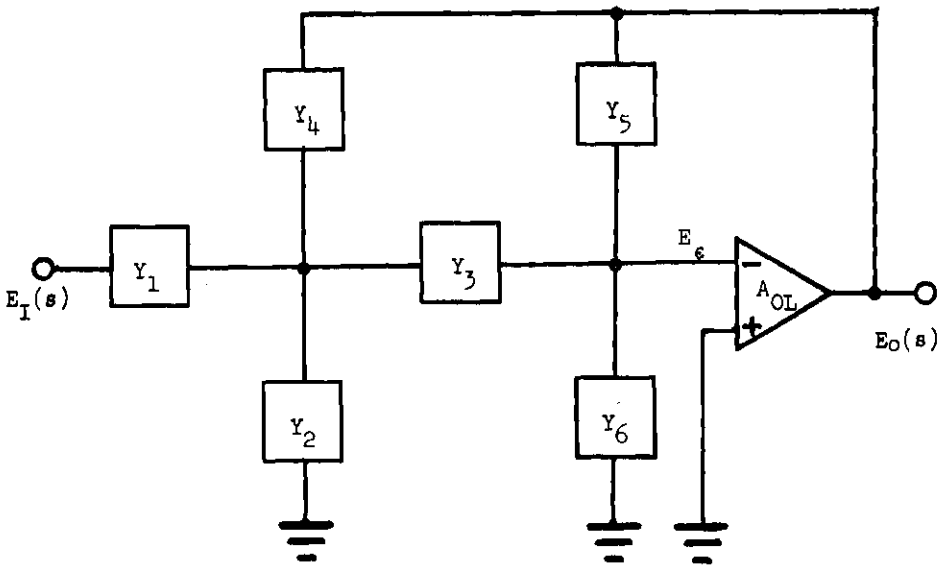

Figure 5. Multiple Inverse Feedback Filter Admittance Diagram.

The general transfer function approaches the ideal response $A_I(s)$ given below whenever the second term in the denominator of (61) is negligible in comparison to the first term.

$$A_I(s) = \frac{-Y_1 Y_3}{(Y_1 + Y_2 + Y_3 + Y_4)Y_5 + Y_3 Y_4} \tag{63}$$

$$= \frac{-s\,\frac{1}{R_1 C_2}}{s^2 + \frac{s}{R_5}\,\frac{1}{C_1} + \frac{1}{C_2} + \frac{1}{R\,R_5 C_1 C_2}} \tag{64}$$

where

$$R = R_1 || R_2 = R_1 R_2/(R_1 + R_2)\ . \tag{65}$$

Comparing this to the standard form (12) gives the design parameters in terms of the component values. In order to use the largest number of standard value components, the two capacitors are chosen to be equal ($Y_3 = Y_4 = sC$) leading to the second form in the equations for the design parameters given by

$$\omega_o^2 = 1/(R\ R_5 C_1 C_2) = 1/(R\ R_5 C^2) \ , \tag{66}$$

$$\delta = 1/Q = (\sqrt{(C_1/C_2)} + \sqrt{(C_2/C_1)})\ \sqrt{(R/R_5)} = 2\sqrt{(R/R_5)} \ , \tag{67}$$

$$A_o = - R_5/(R_1(1 + C_2/C_1)) = - R_5/(2R_1) \ . \tag{68}$$

The inverse of equations (66, 67, 68) gives the circuit reciprocal time constants in terms of the design parameters,

$$1/(R_1 C) = - A_o\ \delta\omega_o \ , \tag{69}$$

$$1/(R_2 C) = (2 - (-A_o)\delta^2)\omega_o/\delta \ , \tag{70}$$

$$1/(R_5 C) = \delta\omega_o/2 \ . \tag{71}$$

While these design equations suffice for filters with $Q < 5$ and with $A_{OL} > 60$ db, they must be modified for those cases which are outside these limits. Again setting the two capacitors equal (61) can be rewritten as

$$A(s) = \frac{- Y_1\ Y_3}{(Y_1+Y_2+2Y_3)(Y_5(A_{OL}+1)+Y_6)/A_{OL}+(Y_1+Y_2)Y_3/A_{OL}+Y_3^2(1+1/A_{OL})} \tag{72}$$

where comparison with the standard equation (12) gives

$$\delta\omega_o A_o = \frac{A_{OL}}{A_{OL} + 1} \frac{1}{R_1 C} \quad , \tag{73}$$

$$\delta\omega_o = \frac{2}{R_5 C} \left[1 + \frac{R_5}{2R(A_{OL} + 1)} + \frac{R_5}{R_{IN}(A_{OL} + 1)} \right] \quad , \tag{74}$$

$$\omega_o^2 = \frac{1}{R\, R_5 C^2} \left[1 + \frac{R_5}{R_{IN}(A_{OL} + 1)} \right] \quad . \tag{75}$$

In order to determine the effect of finite open loop gain on the design, a worst case example is taken to be a filter with Q of 9.08 centered on a frequency of 1 kHz and having a midband gain of 2.00. The open loop gain characteristics of an operational amplifier can be expressed as

$$A_{OL}(f) = |A_{OL}(f)| e^{i\theta(f)} \tag{76}$$

where the open loop voltage gain $|A_{OL}(f)|$ is in db and the phase response $\theta(f)$ is in degrees. Figure 6 shows these characteristics for the 741 along with those for the LM101A with feedforward compensation. Using R_{IN} equal to 2 Megohms for the 741 amplifier, and R_5 less than 0.5 Megohm the two correction terms in equations (74) and (75) are

$$\frac{R_5}{2R(A_{OL} + 1)} \approx \frac{2Q^2}{(A_{OL} + 1)} = 0.165 \angle 90^\circ \quad , \tag{77}$$

and

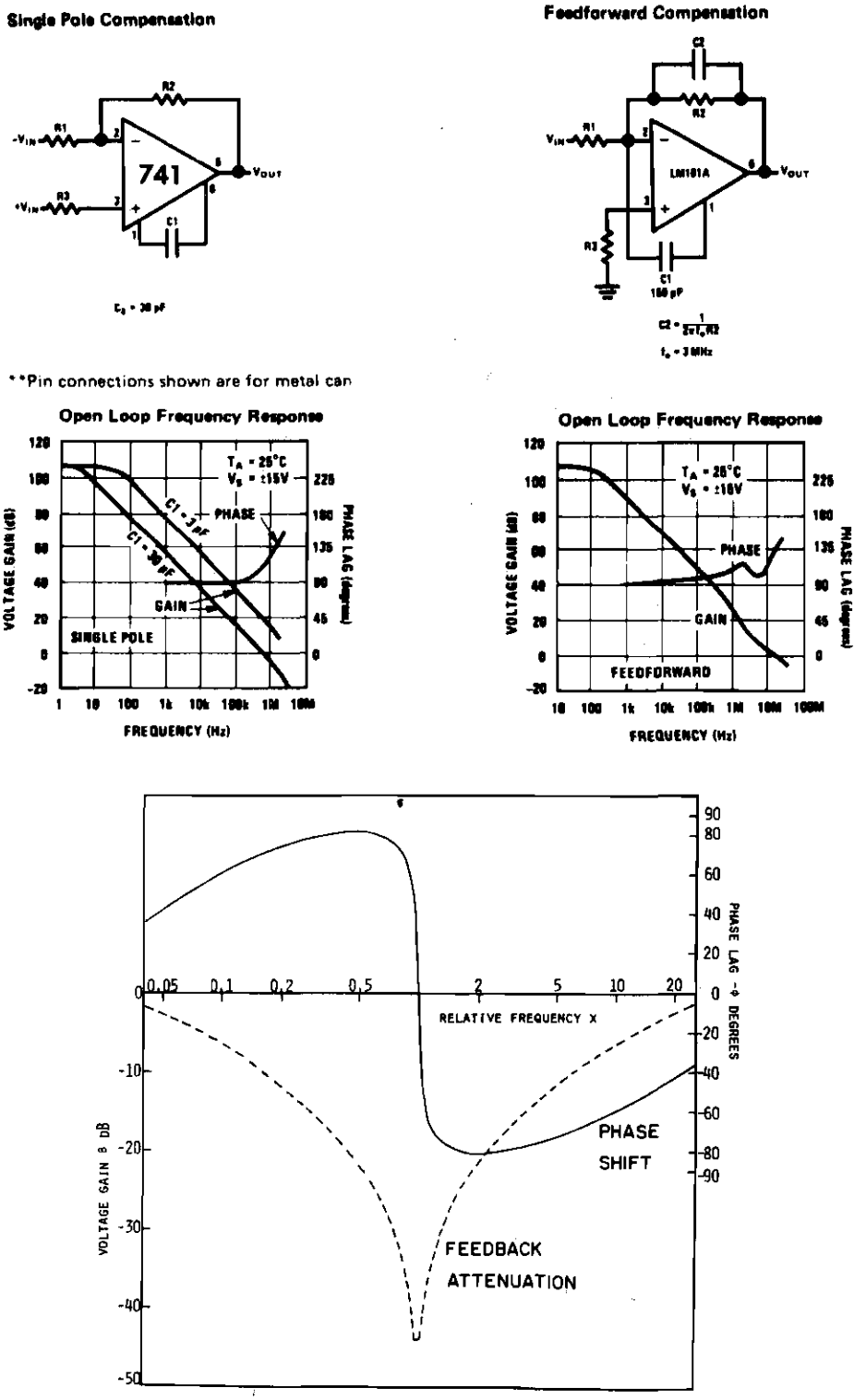

Figure 6. Gain-Phase Frequency Response of Two Operational Amplifiers and Feedback Attenuation Factor β.

$$\frac{R_5}{R_{IN}(A_{OL} + 1)} < 2.5 \times 10^{-4} \angle 90° \tag{78}$$

By neglecting the second term involving the amplifier input resistance the resonant frequency in (75) remains fixed while the damping term δ in (74) and the midband gain A_o in (73) have become complex quantities. This complication is also introduced into the modified design equations obtained by solving equations (73, 74, 75) for the circuit reciprocal time constraints

$$\frac{1}{R_1 C} = \frac{\delta\omega_o (-A_o) A_{OL}}{A_{OL} + 1} \quad , \tag{79}$$

$$\frac{1}{R_2 C} = \frac{\omega_o}{\delta}\left[\frac{2}{\gamma} - \frac{(-A_o)\delta^2 A_{OL}}{A_{OL} + 1}\right] \quad , \tag{80}$$

$$\frac{1}{R_5 C} = \frac{\omega_o \delta}{2}\left[\gamma - \frac{2}{R_{IN} C \omega_o (A_{OL} + 1)\delta}\right] \quad , \tag{81}$$

where

$$\gamma = \frac{1}{2}\left[1 + \sqrt{1 - \frac{8}{\delta^2 (A_{OL} + 1)}}\right] \quad . \tag{82}$$

Since A_{OL} has a large magnitude, these equations reduce to the previous time constant expressions (69, 70, 71) everywhere except for the γ term. For this example, the value of γ is $1.036 \angle -8.7°$ which indicates that purely resistive values of R_2 and R_5 will not give the desired phase and amplitude response. The phase response is less important than the

amplitude response because the detector averages over the phase. Assuming the initial equations (69, 70, 71) are used in the design of the filter, the effect of A_{OL} on the accuracy with which the magnitude of the filter response (63) is realized as well as the effect on the stability of the filter will depend on the loop gain of the filter. The loop gain is defined in Figure 7 which shows the feedback network separated into equivalent attenuation networks $\alpha(s)$ and $\beta(s)$ through which the input and feedback signals are applied to the summing junction at the inverting terminal of the amplifier. Solution of equations (83) and (84) give the system transfer function in terms of attenuation parameters and the open loop gain of the amplifier

$$A(s) = \frac{-\frac{\alpha(s)}{\beta(s)}}{1 - \frac{1}{A_{OL}(s)\beta(s)}} \tag{85}$$

Since this approaches the ideal response for increasing open loop gain, this expression can be written

$$A(s) = \frac{A_I(s)}{1 - \frac{1}{A_{OL}(s)\beta(s)}} \quad . \tag{86}$$

The feedback attenuation factor $\beta(s)$ can now be determined from equation (61) to be

$$\frac{1}{\beta(s)} = 1 - A_I(s)\left[1 + \frac{Y_2}{Y_1} + \frac{Y_6}{Y_1 Y_3}(Y_1 + Y_2 + 2Y_3)\right] \quad . \tag{87}$$

Again, disregarding the amplifier input admittance Y_6 term, this becomes

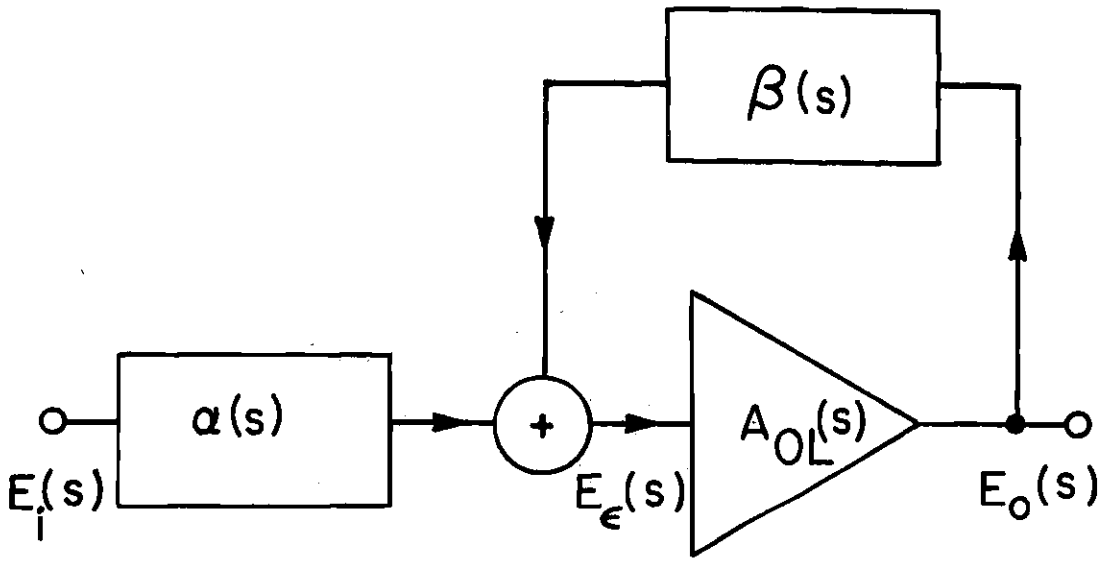

$$E_{\varepsilon}(s) = \alpha(s)\, E_i(s) + \beta(s)\, E_o(s) \tag{83}$$

$$E_o(s) = A_{OL}(s)\, E_{\varepsilon}(s) \tag{84}$$

where

$E_i(s)$ = transformed input signal

$E_o(s)$ = transformed output signal

$E_{\varepsilon}(s)$ = transformed error voltage at input of the amplifier

$A_{OL}(s)$ = open loop transfer function of inverting amplifier

$\alpha(s)$ = input network transfer function

$\beta(s)$ = feedback network transfer function

Figure 7. General Feedback Amplifier Diagram.

$$\beta(s) = \frac{1 + 2RCs + RCR_5Cs^2}{1 + (2RC + R_5C)s + RCR_5Cs^2} \tag{88}$$

For a steady state sinusoidal signal of frequency ω or relative frequency

$$x = \frac{\omega}{\omega_o} \tag{89}$$

the generalized frequency s is replaced by $i\omega$ giving the magnitude and phase angle ϕ of the feedback attenuation network

$$|\beta(ix)| = \sqrt{\frac{(1 - x^2)^2 + (\delta x)^2}{(1 - x^2)^2 + ((\delta + 2/\delta)x)^2}} \tag{90}$$

$$\phi(x) = \text{Arg } \beta(ix) = - \tan^{-1}\left[\frac{2x(1 - x^2)/\delta}{(1 - x^2)^2 + 2(1 + \delta^2/2)x^2}\right] . \tag{91}$$

These functions are shown in Figure 6 for the worst case example. Maximum attenuation of the feedback signal occurs at resonance where the phase shift is zero and the attenuation is

$$|\beta(i\omega_o)| = \frac{\delta^2}{2 + \delta^2} . \tag{92}$$

The maximum phase lag of the network, $\phi(x_-)$ occurs below resonance at the relative frequency

$$x_- = ((2 + \delta^2/2) - \sqrt{(2 + \delta^2/2)^2 - 1})^{\frac{1}{2}} \tag{93}$$

where

$$\phi(x_-) = -\tan^{-1}\left[\frac{1}{\delta\sqrt{2+\delta^2}}\right] . \qquad (94)$$

An equal phase lead occurs at the relative frequency x_+ which is the reciprocal of x_-. In Figure 8 the maximum attenuation and phase lag are shown for a range of common network Q values.

The worst case deviation of the transfer function from $A_I(s)$ in equation (86) exists at resonance where the loop gain $A_{OL}\beta$ is at a minimum due to the dip in $|\beta|$. The phase angle of the loop gain at resonance is approximately -90° due to the phase lag in the amplifier giving

$$|A(i\omega_o)| = \frac{|A_I(i\omega_o)|}{\sqrt{\left(1+\frac{1}{|A_{OL}\beta|^2}\right)}} . \qquad (95)$$

For the 741 example the maximum error is

$$|A(i\omega_o)| = \frac{A_o}{1.014} \qquad (96)$$

giving a 1.4% error. As a practical matter, errors this small are less than those which arise through the use of standard 5% tolerance component values in which case this error may be accounted for in the tuning procedure.

The conditions for instability in the filter are investigated through the use of the stability criterion developed by Nyquist [29]. If plus and minus the imaginary part of $A_{OL}\beta(i\omega)$ is plotted against the real part for frequencies from 0 to ∞, and if the point 1 + i0 lies

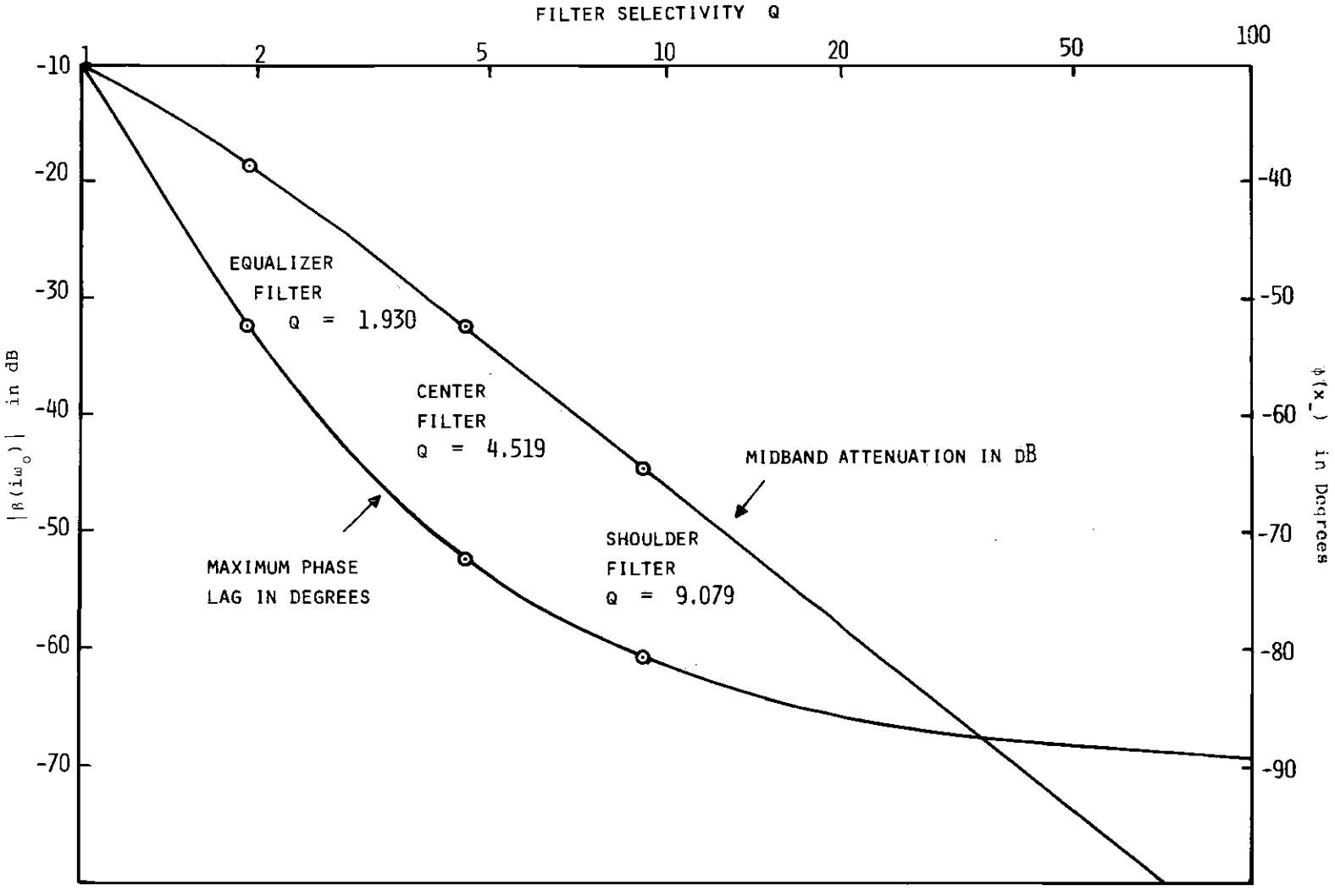

Figure 8. Midband Attenuation and Phase Lag of Multiple Inverse Feedback Filter Versus Selectivity Q.

completely outside this curve, the system is stable; if not it is unstable. The given point is said to lie inside the loop gain curve if a straight line connecting it to the loop gain for frequency f goes through a net angle change when the frequency changes from $-\infty$ to ∞ which corresponds to the point at the origin. In Figure 9, the effect of excessive phase lag in the amplifier causes the loop gain to bend counterclockwise towards the point (1,0), almost encircling it in the center diagram. This situation is conditionally stable because it exhibits positive feedback for a band of frequencies below resonance while the gain around the loop of the inverting amplifier and feedback network is greater than one. If the filter is tuned into this situation, it will be stable until the power is turned off and then back on. A_{OL} increases until the curve encloses the point (1,0) and the amplifier oscillates. This behavior can be avoided and usable accuracy in the magnitude of the response can be achieved if an operational amplifier is used with sufficient open loop voltage gain to give at least 15 dB of loop gain at resonance while maintaining a phase lag θ less than 100° for all frequencies below resonance. This limits the high Q(= 9.079) to 1 kHz for the 741 amplifier and to 20 kHz for the LM101A amplifier with feedforward compensation.

Since only the 741 was available at the time of construction of the filter set, the Wien Bridge filter was chosen for the frequencies above 1 kHz. Figure 10 shows the general admittance diagram for the filter built around an ideal current amplifier which has gain K, zero input impedance and infinite output impedance. The actual current amplifier is shown below this diagram. The transfer function is

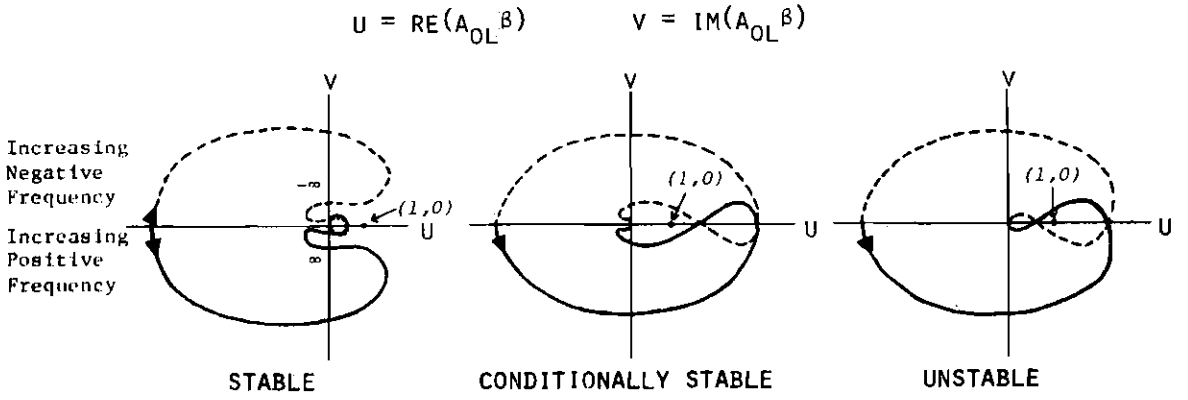

Figure 9. Nyquist Diagram for Multiple Feedback Filter with Operational Amplifier Phase Lag Increasing from Left to Right.

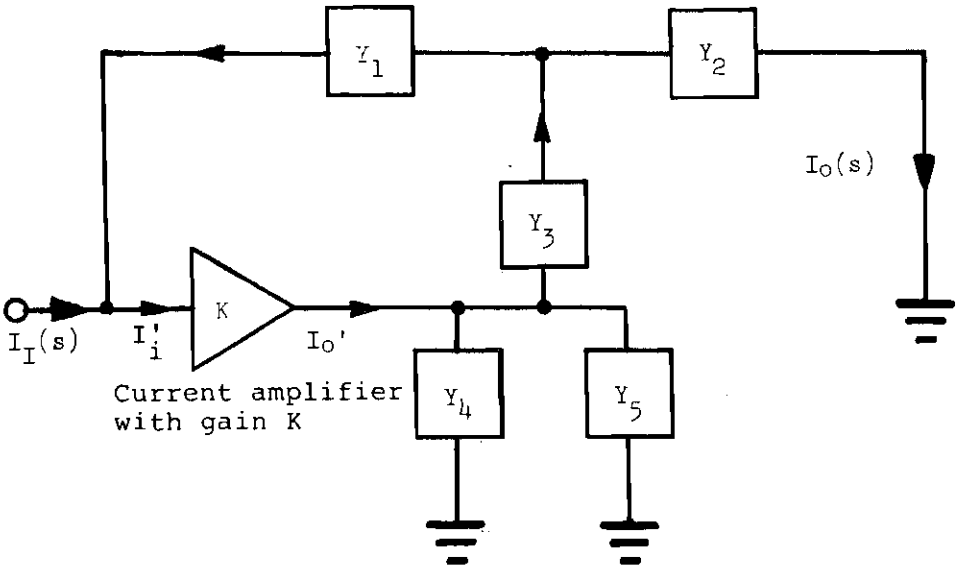

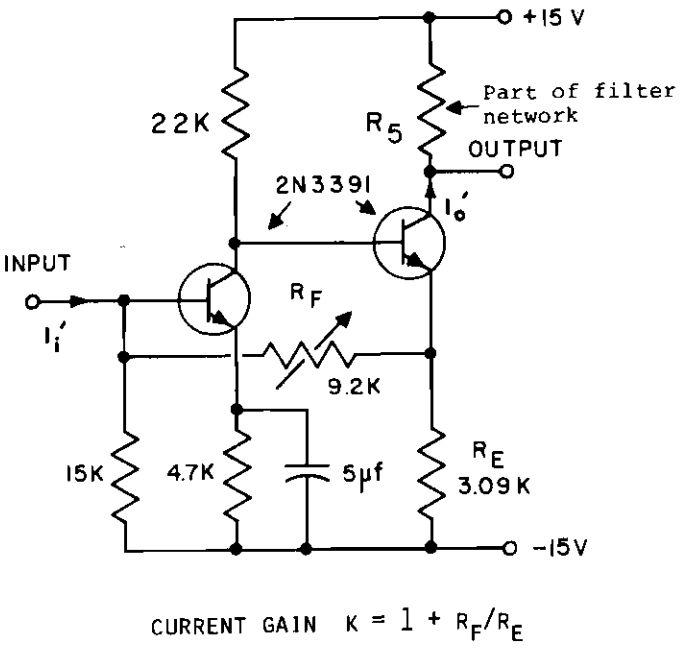

CURRENT GAIN $K = 1 + R_F/R_E$

Figure 10. Admittance Diagram and Current Amplifier for Wien Bridge Filter.

$$A(s) = \frac{K\, Y_2\, Y_3}{(Y_1 + Y_2 + Y_3)(Y_4 + Y_5) + Y_3(Y_1(1 - K) + Y_2)} \quad . \tag{97}$$

If the same admittance parameters in equations (62) are used, then the bandpass parameters can be written as

$$A_o = \frac{K \dfrac{C_3}{C_4} \dfrac{R}{R_2}}{1 + \dfrac{C_3}{C_4}\left\{1 + R\left\{\dfrac{1}{R_5} - \dfrac{K}{R_1}\right\}\right\}} \quad , \tag{98}$$

$$\delta = \frac{1}{Q} = \frac{1 + \dfrac{C_3}{C_4}\left\{1 + R\left\{\dfrac{1}{R_5} - \dfrac{K}{R_1}\right\}\right\}}{\left(\dfrac{R}{R_5}\right)^{\frac{1}{2}} \left(\dfrac{C_3}{C_4}\right)^{\frac{1}{2}}} \quad , \tag{99}$$

$$\omega_o = (R\, R_5 C_3 C_4)^{-\frac{1}{2}} \quad . \tag{100}$$

Again setting the two capacitors equal to C gives the circuit reciprocal time constants

$$\frac{1}{R_1 C} = \frac{2\omega_o}{(A_o - 1)\ \delta(\lambda - 1)} - \frac{A_o \delta \omega_o}{K} \quad , \tag{101}$$

$$\frac{1}{R_2 C} = \frac{A_o \delta \omega_o}{K} \quad , \tag{102}$$

$$\frac{1}{R_5 C} = \frac{(A_o - 1)\ \delta\omega_o(\lambda - 1)}{2} \quad , \tag{103}$$

where

$$\lambda = \sqrt{1 + \frac{4(K - 2)}{2(A_o - 1)^2}} \quad . \tag{104}$$

For the component values in Figure 10, the current gain K is 4.0. If the current gain is increased further, then oscillations will occur due to the positive feedback of the Wien Bridge. The current gain at which this occurs may be calculated by finding the value for which the filter damping term in equation (99) becomes zero. This gives

$$K = \frac{2R_1}{R} + \frac{R_1}{R_5} = 4.16 \tag{105}$$

for the high selectivity shoulder filters. Since the filter operates with a gain close to this critical value, a stable current amplifier is required. The series shunt design shown in Figure 10 provides the necessary stability through the use of negative feedback and metal film resistors for the gain determining components R_F and R_E.

Detection of Narrow Band Noise

The purpose of the detector is to rectify the narrow band noise from each one third octave filter thereby producing a new signal which contains the desired mean square or mean absolute value D.C. component along with bands of frequencies centered on harmonics of the filter mid-band frequency. The location and strength of these components depends on the details of the nonlinear response of the detector. All but a part of the lowest band are then removed by a low pass smoothing filter which transmits the D.C. component along with a slowly varying random signal having a Gaussian amplitude distribution. The uncertainty which

these fluctuations cause in the D.C. component are investigated for both linear absolute value and square law detectors. Finally the percentage fluctuations will be related to the noise bandwidth and the averaging filter time constants.

Unlike the case of a linear device like the one third octave bandpass filter, there is no simple relation such as equation (1) between the detector input and the output power spectrums. This is because the nonlinearity of the detector mixes the input frequency components forming intermodulation distortion products which cannot be described by a linear superposition of the input waves. Instead, the problem can be solved by using the autocorrelation method of North and Van Vleck [30] which is based on the fundamental result that the autocorrelation and the power spectral density of a signal are each a Fourier transform of the other. In both the linear and square law rectifiers, the output autocorrelation $\Psi(\tau)$ can be written in terms of the input autocorrelation $\psi(\tau)$ thus giving an indirect link between the respective power spectrums.

The autocorrelation (or simply correlation) $\psi(\tau)$ of the narrow band noise $V_n(t)$ may be defined as the product of the signal value at a given time t and the value τ seconds later when averaged over all instants of time. In the case of random noise, there is no explicit functional dependence of the signal on time so the concept of ensemble averages will be used. Assuming that a very large collection of identical noise sources exists which is indexed by a sequence of integers and that the i-th source produces a random signal $V_i(t)$ which is uncorrelated with the rest of the sources and if the various statistical

averages of $V_i(t)$ are independent of time, then the instantaneous quantity $V_i(t)\ V_i(t+\tau)$ when averaged for all the sources at the same time t is called the ensemble average correlation function. For a common class of random signals called ergodic processes, [31] of which Gaussian random noise is an example, the time average and ensemble average of the correlation are the same and are indicated by

$$\psi(\tau) = \overline{V_n(t)\ V_n(t+\tau)} = \langle V_i(t)\ V_i(t+\tau)\rangle \tag{105}$$

where the bar indicates a time average and the brackets mean an ensemble average. Several properties of the correlation function may now be derived from this definition,

$$\begin{aligned} \psi(-\tau) &= \psi(\tau) \quad , \\ |\psi(\tau)| &\leq \psi(0) \quad , \\ \psi(0) &= \overline{V_n(t)^2} \quad . \end{aligned} \tag{106}$$

Thus the correlation is an even function of the delay time τ, and is bounded in absolute value by $\psi(0)$ which represents the average power the noise would dissipate in a resistance of one ohm.

The power spectral density $G(f)$ may now be related to the correlation by means of the Fourier transform pair

$$G(f) = \int_{-\infty}^{\infty} \psi(\tau)\ e^{-i2\pi f\tau} d\tau \tag{107}$$

$$\psi(\tau) = \int_{-\infty}^{\infty} G(f)\ e^{i2\pi f\tau} df \quad . \tag{108}$$

Defined in this way, G(f) is also a real, even function of the frequency and is therefore called the two-sided power spectral density. For positive frequencies it has half the value of the one-sided power spectral density where the remaining power is associated with the negative frequencies. Special consideration must be given to D.C. and sinusoidal signals in this treatment because they represent an infinite amount of energy and are characterized by a divergence of the power spectrum integral (107). Nevertheless, these signals contain finite average power and can be incorporated into the formalism by means of the unit impulse $\delta(f)$ defined by

$$\delta(f) = \int_{-\infty}^{\infty} e^{-i2\pi f\tau}\, d\tau \tag{109}$$

and

$$g(f_o) = \int_{-\infty}^{\infty} g(f)\, \delta(f - f_o)\, df \quad . \tag{110}$$

This impulse is used to indicate that a non-zero amount of signal power is concentrated at a specific frequency. For example, if

$$V(t) = A + B \cos 2\pi f_o t \tag{111}$$

then

$$\psi(\tau) = A^2 + (1/2)\, B^2 \cos 2\pi f_o \tau \tag{112}$$

leading to

$$G(f) = A^2\, \delta(f) + (B^2/4)\, \delta(f - f_o) + (B^2/4)\, \delta(f + f_o) \quad . \tag{113}$$

This indicates that the D.C. power at zero frequency is A^2 while one half the average power $B^2/2$ is associated with the frequencies f_o and $-f_o$.

Next, assuming that the filtered noise signal $V_n(t)$ has a Gaussian amplitude distribution with autocorrelation $\psi(\tau)$ (or ψ_τ for short), then the joint probability distribution of $V_1 = V_n(t)$ and $V_2 = V_n(t + \tau)$ is given by the Bivariate Normal distribution,

$$P(V_1,V_2) = \frac{1}{2\pi(\psi_o^2 - \psi_\tau^2)^{\frac{1}{2}}} \exp\left[\frac{-(\psi_o^2 V_1^2 + \psi_o V_2^2 - 2\psi_\tau V_1 V_2)}{2(\psi_o^2 - \psi_\tau^2)}\right] . \qquad (114)$$

This expresses the probability of measuring the voltages V_1 and V_2 at times t and $t + \tau$ for each noise source in the given ensemble. The output correlation for the general rectifier with output voltage $V(t) = F[V_n(t)]$ may then be written as

$$\psi(\tau) = \langle F[V_1]F[V_2]\rangle = \int_{-\infty}^{\infty} dV_1 \int_{-\infty}^{\infty} dV_2 F[V_1]F[V_2]P(V_1,V_2) . \qquad (115)$$

An outline of this integration is given in Appendix A for the linear and square law detectors following a procedure discussed by Rice [32]. The output correlations are listed here below each rectifier response function. First, for the linear full wave rectifier

$$F[V_n(t)] = \alpha|V_n(t)| , \qquad (116)$$

and

$$\psi_L(\tau) = (2/\pi)\alpha^2\psi_o \left[(1 - \rho^2)^{\frac{1}{2}} + \rho(\cos^{-1}(-\rho) - \frac{\pi}{2})\right] , \qquad (117)$$

where $\rho \equiv (\psi_\tau/\psi_o)$ is the normalized correlation variable. Secondly, for the square law device

$$F[V_n(t)] = \beta V_n(t)^2 \quad , \tag{118}$$

and

$$\psi_S(\tau) = \beta^2 \psi_o^2(1 + 2\rho^2) \quad . \tag{119}$$

In Figure 11 these two correlations are graphed versus the input correlation ψ_τ. Also shown for comparison is an approximation which takes the first two terms of the Maclaurin series expansion of $\psi_L(\tau)$ given in Appendix A.

$$\psi_L(\tau) = (2/\pi)\alpha^2\psi_o\left[1 + \rho^2/2 + \sum_{n=2}^{\infty} a_{2n}\,\rho^{2n}\right] \tag{120}$$

where

$$a_{2n} = \frac{(2n - 3)!!}{(2n)!!(2n - 1)} \quad . \tag{121}$$

Of interest in Figure 11 are the correlations for $\tau = 0$ which give the total average power, and the correlations as $\tau \to \infty$ which give the power due to the D.C. component in the signals. These values are listed in Table 4 along with the uncertainty in the D.C. output for input noise with bandwidth B and the D.C. output for sinusoidal input. Note that the average power and D.C. power are proportional to the input noise power ψ_o for the linear case, and vary as the square of the input power for the square law case. The linear detector approximation

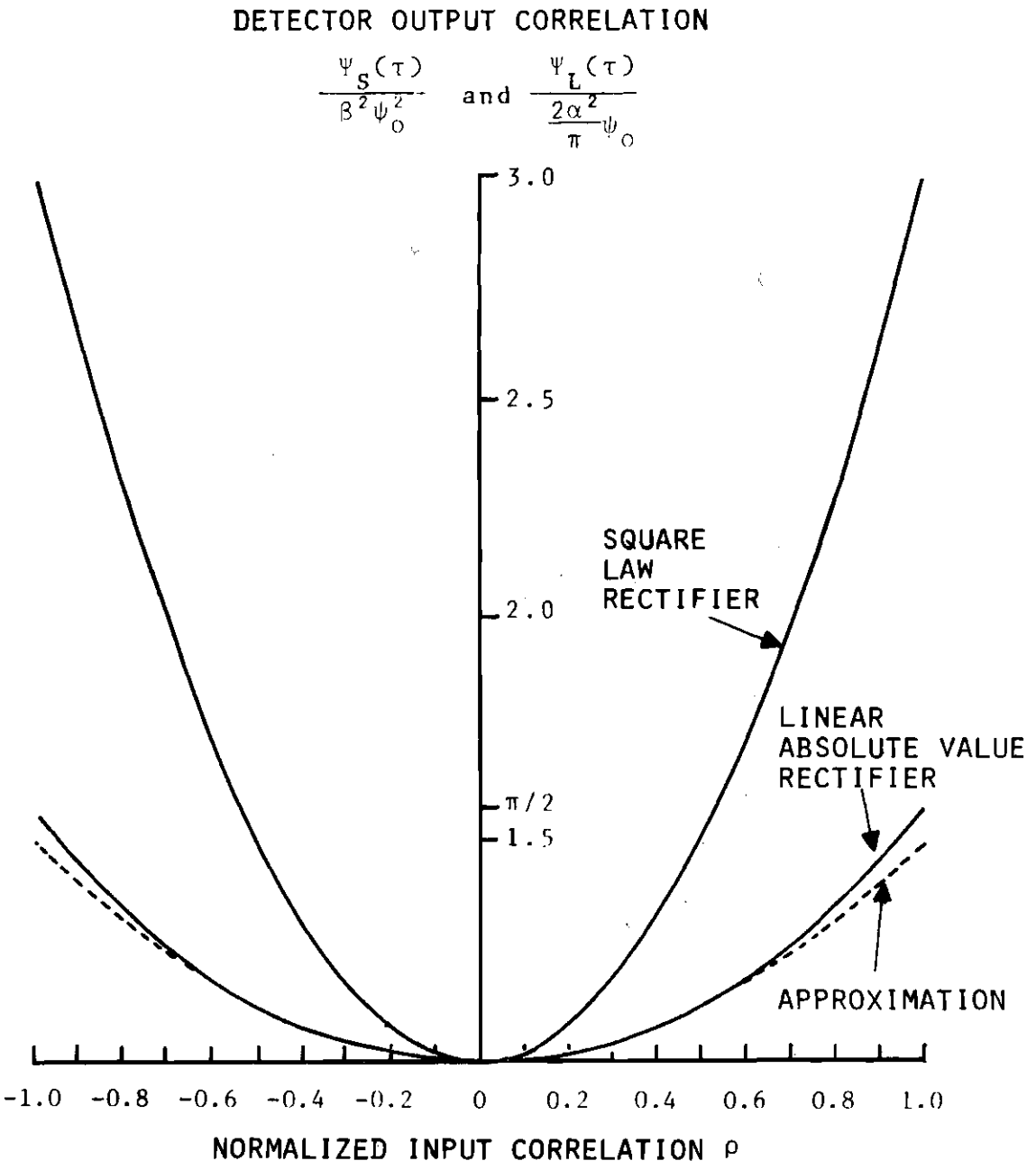

Figure 11. Normalized Detector Output Correlations Versus Correlation of Narrow Band Input Noise.

Table 4. Statistical Quantities for the Output of the Absolute Value Linear and Square Law Detectors with Narrow Band Noise and Sinusoidal Inputs

Quantity	Narrow Band Input Noise	Square Law Detector	Linear Detector	Linear Approximation
Correlation at $\tau = 0$ total average power	ψ_o	$3\beta^2\psi_o^2$	$\alpha^2\psi_o$	$(3/\pi)\alpha^2\psi_o$
Correlation as $\tau \to \infty$ D.C. output power	0	$\beta^2\psi_o^2$	$(2/\pi)\alpha^2\psi_o$	$(2/\pi)\alpha^2\psi_o$
Mean D.C. output	0	$\beta\psi_o$	$(2/\pi)^{1/2}\alpha\psi_o^{1/2}$	$(2/\pi)^{1/2}\alpha\psi_o^{1/2}$
δ = uncertainty in detector mean output	—	$2\sqrt{1/8BRC}$	$\sqrt{1.056/8BRC}$	$\sqrt{1/8BRC}$
Detector mean output for sinusoidal input $A \cos 2\pi f_o t$	—	$(1/2)\beta A^2$	$(2/\pi)\alpha A$	—

underestimates the average power by 4.5% because the series truncation neglects the power due to modulation products higher than second order.

The series expansion for the linear output correlation, equation (120) may be used to calculate the output spectrum by taking the Fourier transform of each term individually and by summing the results. The linear approximation $G_A(f)$ involves only the first two terms. This involves consideration of integrals of the form

$$G_{2n}(f) = \int_{-\infty}^{\infty} \psi_\tau^{2n} \, e^{-i2\pi f\tau} \, d\tau \ . \tag{122}$$

They may either be integrated directly, or else expressed as the 2n - 1 fold convolution of the applied noise spectrum G(f) with itself. That is, ψ_τ^{2n} may be factored to give

$$G_{2n}(f) = \int_{-\infty}^{\infty} \psi_\tau^{2n-1} \, \psi_\tau \, e^{-i2\pi f\tau} \, d\tau = G_{2n-1}(f) * G(f) \ , \tag{123}$$

where

$$G_{2n-1}(f) * G(f) \equiv \int_{-\infty}^{\infty} G_{2n-1}(f') \, G(f - f')df' \ , \tag{124}$$

by the convolution theorem for Fourier integrals. By repeated application of this recursion relation, the desired relation between $G_{2n}(f)$ and G(f) can be found. Generally, however, this convolution approach is only used to estimate the location and shape of the spectral components in $G_{2n}(f)$. For example, if the ideal bandpass filter with white noise input is chosen to give a noise spectrum having bandwidth B, center frequency f_o and spectral density w_o, then $G_2(f)$ has triangular

peaks symmetrical about $\pm 2f_o$ with bandwidth twice that of the input spectrum and a central peak at zero frequency which has the same shape but double the amplitude. Proceeding further with the convolution process shows that for even orders, the peaks of $G_{2n}(f)$ are located on even multiples of f_o and extend to $\pm 2nf_o$. Middleton [33] has shown that these G_{2n} terms correspond to the 2n th order intermodulation distortion products, and that the total power associated with each term depends only on the total input power of the applied noise, not on its spectral distribution. When the detector input consists of relatively narrow frequency bands so that the detector output spectrum consists of bands, Middleton has also shown that the power in each output band depends only on the input noise power and not on the input spectrum. Since the low pass smoothing filter which follows the detector greatly attenuates the higher frequency components, it will only be necessary to consider those terms in the detector output which are concentrated about zero frequency. Continuing with the ideal bandpass filter model, the correlation of the filtered noise is computed from equation (108) to be

$$\psi(\tau) = \psi_o[\sin(\pi B\tau)/\pi B\tau]\cos 2\pi f_o\tau \tag{125}$$

where $\psi_o = w_o B$. The expression for $G_{2n}(f)$ then becomes

$$G_{2n}(f) = {}_o^{2n} \int_{-\infty}^{\infty} \left(\frac{\sin \pi B\tau}{\pi B\tau}\right)^{2n} \cos^{2n}(2\pi f_o \tau)\, e^{-i2\pi f\tau}\, d\tau \tag{126}$$

where it is then noted that the central peak is due to the constant term in the expression

$$\cos^{2n}(2\pi f_o \tau) = 2^{-2n}\left[\sum_{k=0}^{n-1} 2\binom{2n}{k} \cos 2(n-k)2\pi f_o \tau + \binom{2n}{n}\right]. \qquad (127)$$

The other terms in the expansion are responsible for the higher frequency groups centered on multiples of $2f_o$. Finally, setting f = 0 in the integral (126) gives

$$G_{2n}(0) = \psi_o^{2n}(1/B)2^{-2n}\binom{2n}{n} I_{2n} \qquad (128)$$

where

$$I_{2n} = (1/\pi)\int_{-\infty}^{\infty} \left(\frac{\sin x}{x}\right)^{2n} dx \qquad (129)$$

is a constant which decreases slowly with increasing values of n. This integral and an approximation good for large n are given in Appendix A. Also the series for $G_L(0)$ is summed for the first ten terms and is found to be

$$G_L(0) = \psi_o(2/\pi)\alpha^2[\delta(f) + (1/4B)(1.056)] \; . \qquad (130)$$

The impulse located at zero frequency corresponds to the mean value of the output. The number 1.056 indicates the strength of the low frequency power spectrum and agrees with the measurements of 1.06 given by Lawson and Uhlenbeck [34].

The power spectrum for the square law detector can next be calculated using the ideal filter model giving

$$G_S(f) = \beta^2(\psi_o^2\, \delta(f) + 2\, G(f) * G(f)) \; . \qquad (131)$$

The low pass smoothing filter once again limits consideration to the frequencies near zero so that

$$G_S(0) = \beta^2 \psi_o^2 (\delta(f) + \frac{1}{B}) \quad . \tag{132}$$

The low frequency contribution of $G_2(f)$ to the output spectrum of the square law detector $G_S(f)$ and to the linear detector $G_A(f)$ approximation can be calculated for the one third octave filter by convoluting the polynomial response function g(f) with itself in (123). The low frequency spectrum obtained by numerical integration is shown in Figure 12 along with the transfer response for the associated low pass smoothing filter. Since the detector spectrum remains constant over most of the passband of the low pass smoothing filter, it may be assumed constant for all frequencies. Since a narrow band portion of the detector output is taken, the output may be assumed to approach the statistical properties of Gaussian random noise. That is, the instantaneous output is distributed normally about the mean output D.C. value.

It is now possible to formulate an expression for the standard deviation σ of the fluctuations as a function of the one third octave bandwidth and the smoothing filter time constant. For the standard low pass RC filter shown in Figure 13 the amplitude response and output power spectrum are indicated.

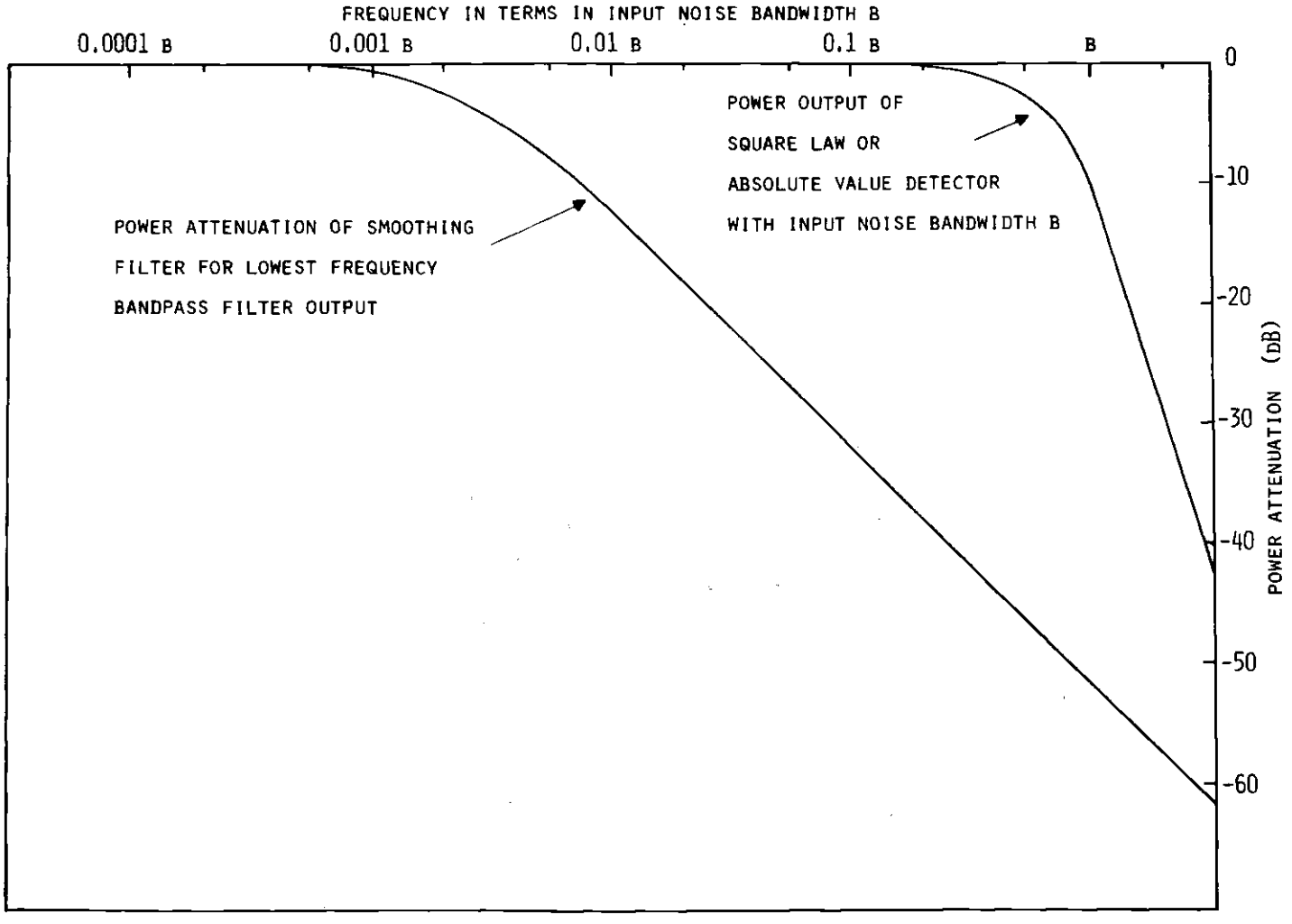

Figure 12. Power Spectrum of Detector Output and Power Attenuation of Smoothing Filter.

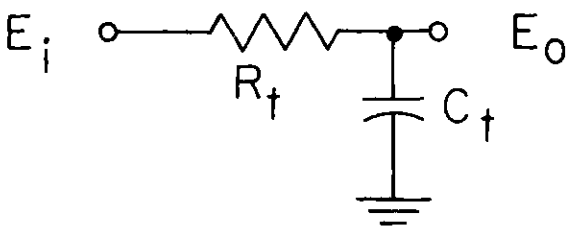

Figure 13. RC Smoothing Filter.

$$|A_{LP}(f)| = \left|\frac{E_o(f)}{E_i(f)}\right| = \frac{1}{[1 + (2\pi f R_t C_t)^2]^{1/2}} \tag{133}$$

The averaging filter power spectrum $G_{LP}(f)$ is determined from the detector power spectrum $G_{Det}(f)$ by equation (1).

$$G_{LP}(f) = |A_{LP}(f)|^2 \, G_{Det}(f) \approx \frac{1}{1 + (2\pi f R_t C_t)^2} \, G_{Det}(0) \tag{134}$$

Integration of this narrow band of noise output power in terms of σ gives

$$\sigma^2 = \int_{-\infty}^{\infty} G_{LP}(f) \, df = \frac{G_{Det}(0)}{2RC} \quad . \tag{135}$$

This gives for the linear detector

$$\sigma_L = (\gamma\alpha^2/4\pi)^{1/2}\left(\frac{\psi_o}{BRC}\right)^{1/2} \tag{136}$$

where $\gamma = 1.056$, and for the square law detector

$$\sigma_S = \frac{\beta \, \psi_o}{\sqrt{(2BRC)}} \quad . \tag{137}$$

A more useful quantity for indicating the uncertainty in the D.C. output caused by these low frequency fluctuations is the fractional uncertainty δ equal to the ratio of the uncertainty to the mean output. These values are listed in Table 4.

While the smoothed output of the linear detector may now be displayed as a measurement for the rms value of the one third octave noise, the square root of the corresponding output of the square law detector must be taken. This may be done directly with a square root circuit, or else may be done by halving the output of the logarithm converter which is used to produce the decibel display. In either case, the uncertainty is also approximately halved in the process, the approximation being particularly good for the 1 to 5% uncertainties encountered in the filter set which was constructed. This is seen by considering

$$\sqrt{(V_S[1 \pm \delta_S])} = V_S^{\frac{1}{2}}(1 \pm \delta_S/2) \tag{138}$$

so that for both linear and converted square law detectors the fractional uncertainty expressed as a percent p is

$$p = \sqrt{\left\{\frac{1250}{BRC}\right\}} \quad . \tag{139}$$

This may be rewritten to give the averaging filter time constant required to produce p% fluctuations for a given bandwidth B of noise

$$RC = \frac{1250}{Bp^2} \quad . \tag{140}$$

Since the worst case situation occurs at the lowest frequency filter

for which the largest time constant is needed, it is necessary to consider the time required for the averaging network to respond to changes in the signal level. That is, as the time constant is increased, the time required for the averaging network to settle to within 5% of the final value is 3RC a value which may become too long for the mean value to be useful as a real time measurement. As a result the lowest three filter time constants were decreased to about 12 seconds giving a compromise percentage fluctuation of 5%. These filter values are listed in Appendix B along with the filter circuit values.

CHAPTER III

INSTRUMENTATION

Figure 14 shows the block diagram of the real time analyzer. The performance of each section will now be discussed. The operational amplifier with an RC feedback network is the basis for implementing the low frequency half of the bandpass filters. When devices such as silicon diodes and transistors are substituted into the feedback loop, the same order of accuracy obtained in approximating the filter response can be extended to the non-linear absolute value and logarithmic responses. Accompanying this discussion of the detector and decibel conversion circuits is a description of the analog multiplexer and associated digital logic control.

The Absolute Value Rectifier

The basic unit [35] in this circuit shown in Figure 15 is a precision limiter or half wave rectifier. This is followed by a summing amplifier which gives the output

$$E_{out} = -(E_i + 2\ E_o)\ , \tag{141}$$

where E_i and E_o are the input and output voltages of the limiter. The two diodes are included in the feedback loop of amplifier A_1 in order to reduce the influence of their non-ideal switching characteristics which are described by the diode volt-ampere relation [36],

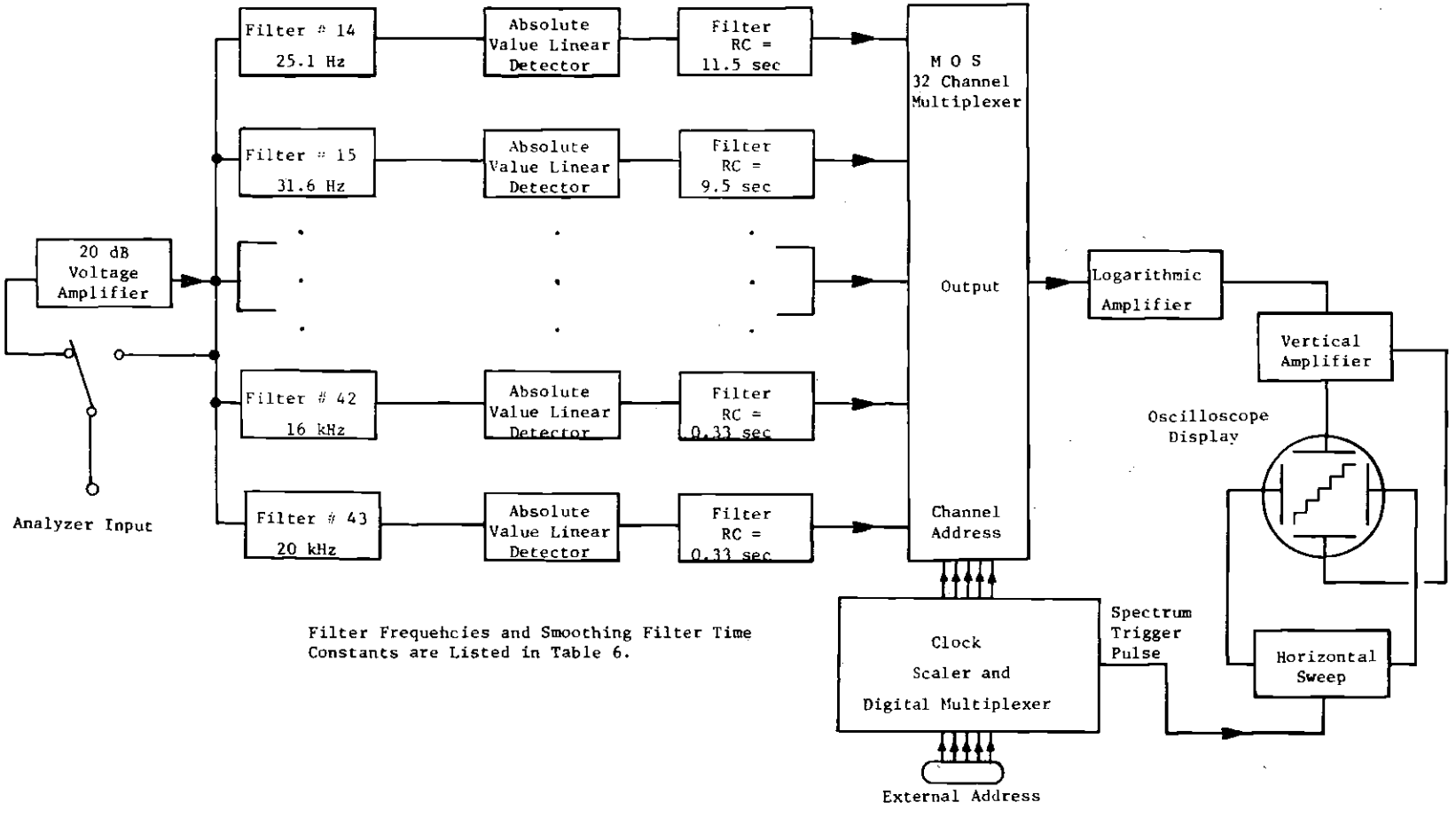

Filter Frequehcies and Smoothing Filter Time Constants are Listed in Table 6.

Figure 14. Block Diagram of Real Time Audio Analyzer.

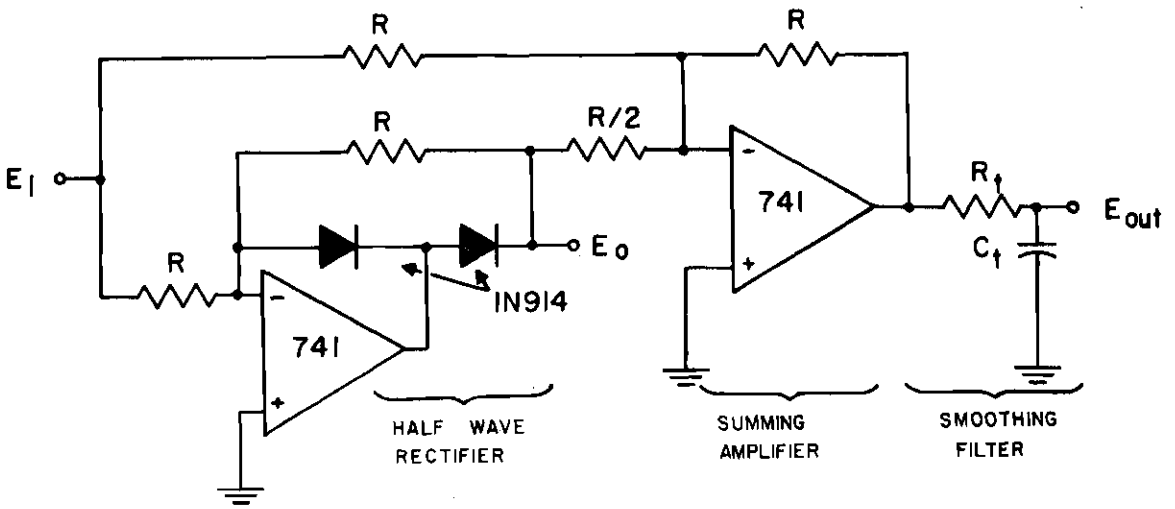

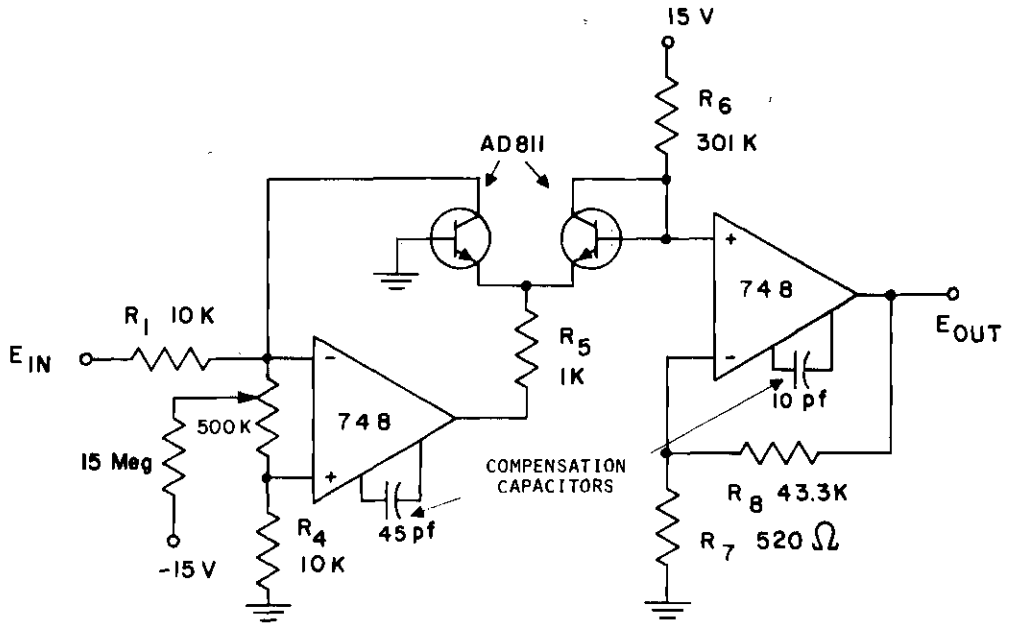

THE 748 AMPLIFIER IS SIMILAR TO THE 741 EXCEPT THAT THE COMPENSATION CAPACITOR IS APPLIED EXTERNALLY.

Figure 15. Circuits for Linear Absolute Value Rectifier and Logarithmic Amplifier.

$$v = f(i) = \frac{kT}{q} \ln \left(\frac{i}{I_o} + 1 \right) , \tag{142}$$

where v = volt drop across diode

i = current flow through diode

k = Boltzmann's constant

q = electron charge

T = Temperature in $^{\circ}k$

I_o = reverse bias saturation current.

For negative input voltages, the limiter operates as a normal inverting amplifier with D_2 reverse biased by the positive output of A_1 which is also feedback to the amplifier input by resistor R_f. By taking into account the finite gain of the amplifier and the diode characteristic in equation (142), the limiter output can be shown to be

$$E_o = \frac{-(R_f/R_i)\ E_i}{1 - \frac{1}{A_{OL}\beta} \left(1 + \frac{f(i_2)}{e_o} \right)} \approx - E_i \tag{143}$$

where

$$\beta = R_1/(R_1 + R_f) = 1/2 \tag{144}$$

is the feedback attenuation factor. This shows that the nonideal behavior of the diode is reduced by the loop gain $A_{OL}\beta$ which is greater than 50 for the 741 amplifier for all frequencies of interest.

For positive input, the negative output of A_1 is disconnected from the output point E_o by reversed biased diode D_1 so all the input

current i_1 flows through diode D_2 thereby clamping the output to -0.6V or $-f(i_1)$. The voltage at the summing junction then produces the negligibly small output

$$E_o = - \frac{f(i_1)}{A_{OL}} \frac{R/2}{R/2 + R_f} \approx 0 \quad . \tag{145}$$

The Logarithmic Amplifier

This circuit described by Widlar and Giles [37] is based on the near logarithmic dependence of the base to emitter voltage V_{BE} on the collector current I_C for transistors with low surface recombination rates,

$$I_C \propto e^{q\, V_{BE}/kT} \tag{146}$$

where

$$V_{BE} > 4\ kT/q = 0.1\ \text{Volt} \ @\ T = 25°C \quad . \tag{147}$$

The exact proportionality constant depends on the base and emitter impurity doping levels which are closely matched in integrated circuit constructions. For such a pair of transistors equation (146) gives the base emitter voltage difference for the two transistors operating at different collector current levels I_{C_1} and I_{C_2},

$$\Delta V_{BE} = V_{BE_1} - V_{BE_2} = \frac{kT}{q} \ln \left(\frac{I_{C_2}}{I_{C_1}} \right) \tag{148}$$

In the circuit shown in Figure 15, negative feedback through transistor

Q_1 causes the input signal current to flow through it giving

$$I_{C_1} = E_{in}/R_{in} \quad . \tag{149}$$

Since Q_1 is connected in the common base configuration, it introduces voltage gain into the feedback loop of amplifier A_1. In order to maintain stability, the loop gain is reduced by inserting resistor R_5 and by increasing the compensation capacitor C_F to 50% above the nominal 30 pF value. The collector current of Q_2 is established by V_+ and R_6 at the reference value

$$I_{c_2} = V_+/R_6 \quad , \tag{150}$$

where the base voltage difference ΔV_{BE} and base current for Q_2 are neglected in comparison to V_+ and I_{C_2} respectively. The base potential of Q_2 is then amplified by the high input impedance non-inverting amplifier A_2 with the gain determined by feedback resistors R_7 and R_8 giving

$$E_{out} = \frac{(R_7 + R_8)}{R_7} (-) \frac{kT}{q} \ln \left(\frac{E_{in}/R_1}{V_+/R_6} \right) , \tag{151}$$

$$= (-)\ 5.04 \text{ Volt } \log_{10} (E_{in}/0.5 \text{ Volt}) \tag{152}$$

where the temperature is taken to be 25°C.

The Multiplexer

The basic unit of the multiplexer is the Fairchild 3705 MOS 8 channel multiplex switch which contains a built-in one-of-eight decoder which decodes a three bit TTL address from the control system and

switches to the corresponding analog channel. In order to switch 32 analog channels Accardi [38] has connected the outputs of four multiplexer chips while driving their output enable lines individually. This is done using the logic which decodes the last two bits, A_3 and A_4 as shown in the truth table in Figure 16.

In order to access the multiplexer at random, or to sample the channels sequentially, additional logic circuits were added as shown in the figure. If the set bit is activated, the address will be supplied directly from an external address source such as a mini-computer; otherwise, the clock driven counter made up of five self-complementing D type flip flops provides the address. This provides for interfacing the analyzer to a computer for analysis and control.

The channel switching time of 1 μsec is negligible in comparison to the 670 μsec channel sampling time. When a switch goes on, the channel resistance goes from over 1.5 Gohm to less than 400 ohms.

A One Third Octave Equalizer

An equalizer was constructed by serially connecting thirty band reject filters having adjustable attenuation [39]. Each reject filter was tuned to a standard one third octave center frequency where it was designed to give an adjustable attenuation of up to -14 dB. For the maximum setting, the attenuation at the nominal one third octave band edge frequencies was chosen to be half this value or -7 dB. The synthesis of this response was accomplished by first bandpass filtering the signal and by then allowing controlled amounts of this filtered signal to destructively interfere with the original input signal. In Figure 17 the summing amplifier adds the input signal E_{in} to a fraction of the

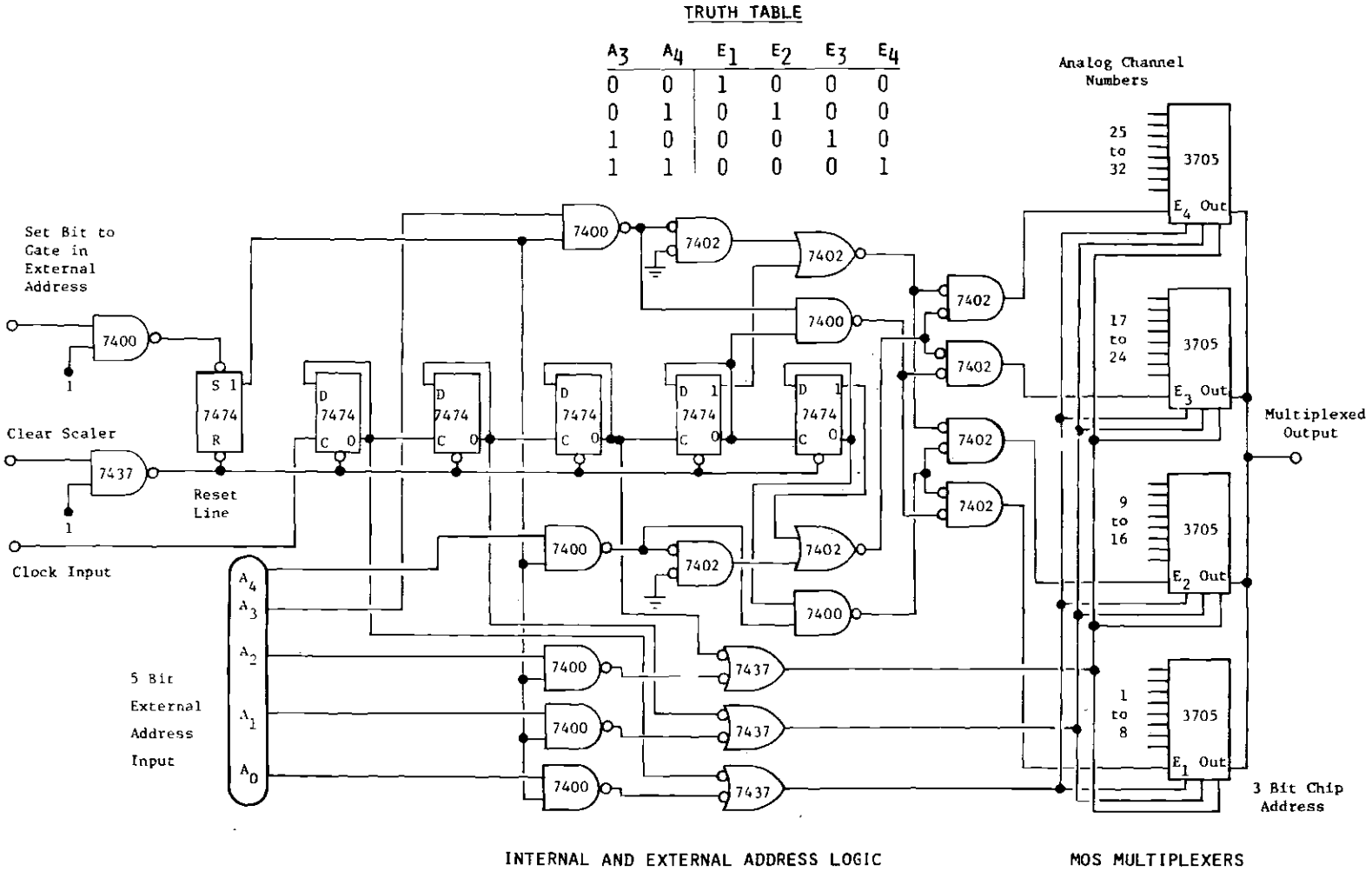

Figure 16. MOS Analog Multiplexer with Associated Logic for Address Selection.

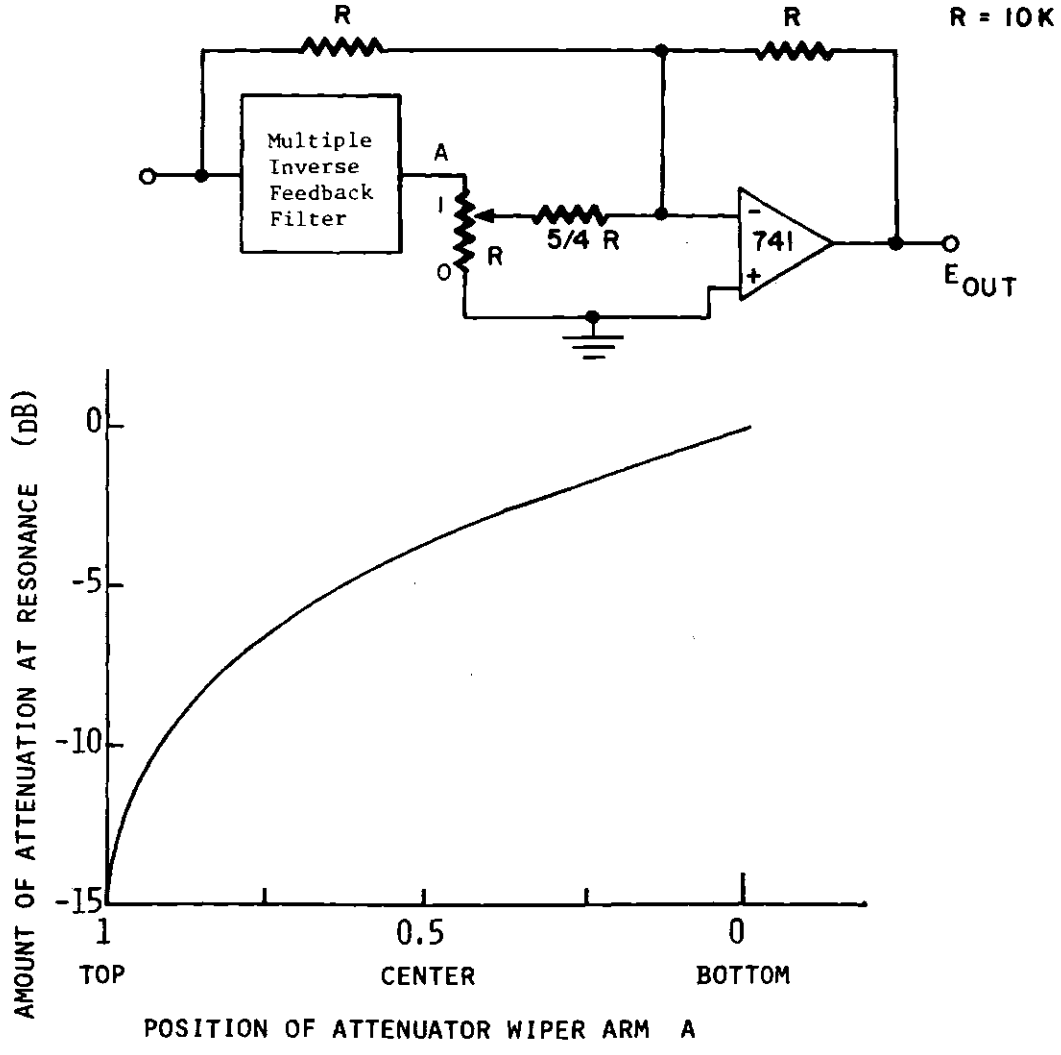

Figure 17. Circuit Diagram and Midband Attenuation Versus Attenuator Position for the Adjustable Band-reject Equalization Network.

filtered output E_o producing the interference signal E_{out}. The fraction is determined by the position parameter a which varies linearly with the position of the wiper arm and has the value 0 when the movable tap is at the bottom and the value 1 when it is at the top. Using the summing resistor values and the multiple inverse feedback bandpass filter with unity gain at the midband frequency, the decibel attenuation at midband is given in terms of the parameter a by

$$\frac{E_{out}}{E_{in}} = 20 \log_{10} \left(\frac{1}{1 + \frac{a}{(5/4) - a^2}} \right) . \qquad (153)$$

The effect of this control on the midband attenuation is shown in Figure 17. The correct bandedge attenuation of -7 dB is obtained with a bandpass filter Q of 1.930. This filter output and the maximum interference output are shown in Figure 18A. Since the required Q is low, (92) indicates that the resulting feedback attenuation factor β is only -30 dB. This means that the filter may be realized for all audio frequencies by using the 741 amplifier since the loop gain would always be greater than 20 dB.

As an indication of the combined action of the rejection networks, six adjacent filters were chosen with different combinations of the attenuator settings. In Figure 18B the dotted curve represents a -2 dB attenuation setting corresponding to an a value of 0.70 for each filter. The average -10 dB response over the range of the filters results from attenuation of the reject networks outside their stop bands. Increasing the attenuation to -14 dB for all filters yields the uneven response shown by the solid curve. The average response of -20 dB is double the

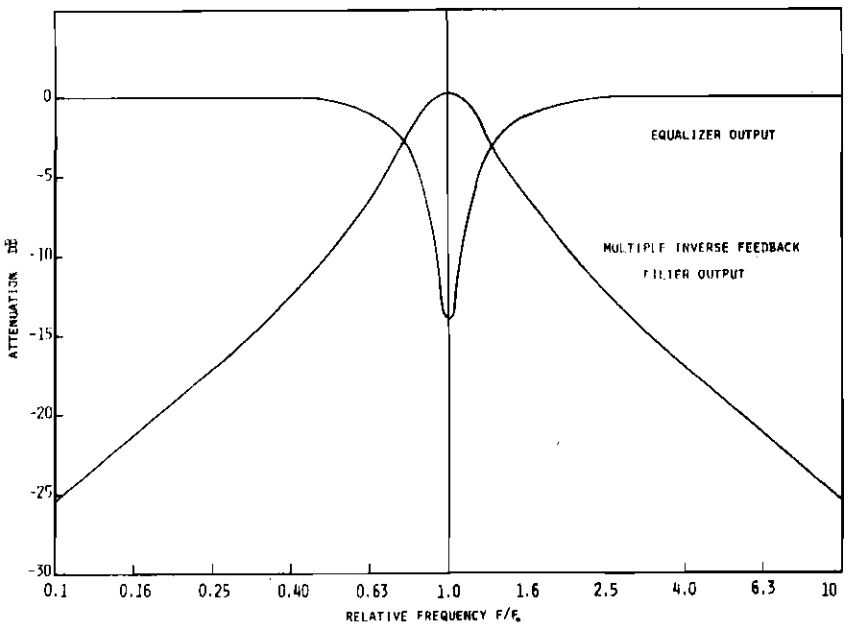

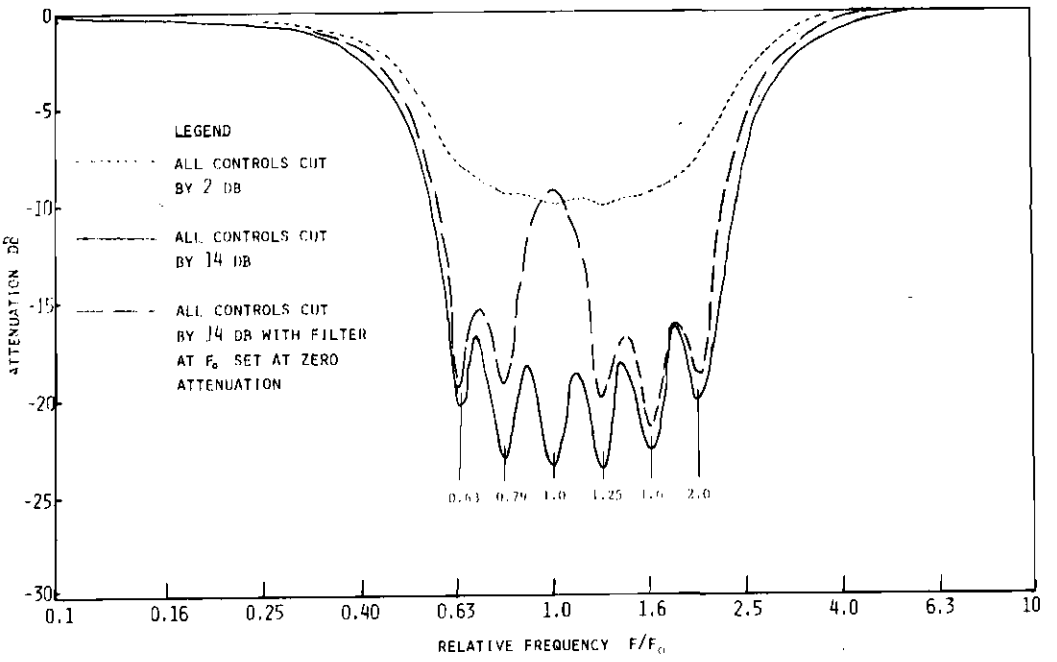

Figure 18. Frequency Response of Single Equalizer with Associated Bandpass Response and Frequency Response of Six Equalizer Filters.

attenuation of the previous settings. Finally, the dashed curve shows the result of removal of the attenuation at one filter frequency. These results show that considerable spectrum equalization can be obtained with only minor influences between adjacent attenuation settings.

CHAPTER IV

EXPERIMENTAL PROCEDURE

Adjustment of Filters

Adjustment of the high and low frequency filters is based on the design equations (69-71) and (101-104). The low frequency filter is easily tuned since R_2 adjusts ω_o while leaving A_o fixed at the value set by R_5. The low output impedance of each operational amplifier serves to isolate the filter from the load so they may be tuned separately and then connected in series for use. In order to prevent overload of succeeding stages, the lowest gain center frequency filter is placed before the higher gain shoulder filters.

The Wien Bridge filter is also easily adjusted since ω_o is independent of the current gain control K. R_1 is first adjusted to resonate the filter at this frequency, then both Q and A_o will be adjusted with K. The exact value of A_o is left undetermined while Q is set according to the result from (18), i.e., for both the center and shoulder filters the response at midband is 33.0 dB above the response at 10 ω_o and $\omega_o/10$.

In the derivation of the Wien Bridge filter, the current signal was assumed to be supplied by an ideal current source, filtered and then supplied to a point which remains at ground potential. Since each filter has a low input impedance of typically 22 ohms due to the internal negative feedback, this appears to be ground for the current supplied by the high output impedance R_2 of the previous filter. The voltage signal is converted into a proportional current by means of a 100 K series

resistor. After filtering, the current is converted back to a voltage by an inverting amplifier with 100 K feedback resistor. The resistor is adjusted to give unity gain at the midband frequency, thus compensating for the arbitrary A_o values of each current filter.

Equalization Procedure

The analyzer is first calibrated by displaying the spectrum of a white noise signal. Since the power transmitted by each filter is proportional to the bandwidth which in turn is a constant fraction of the center frequencies, the power will double for each octave. This means each filter output increases by 1 dB for increasing frequency. The oscilloscope vertical gain and position are adjusted to extend the spectrum over the screen. The level is increased until the noise signal begins to clip in the analyzer preamplifier.

Equalization is accomplished by connecting the analyzer to a General Radio Model 1558 Sound Level Meter and precision 1/2 inch condenser microphone. The loudspeaker and power amplifier are connected to a pink noise source as shown in Figure 19. The gain is increased until the power spectrum is 10 dB greater than the background noise level for all the filter bands. The equalizer is then inserted in the amplifier line with all attenuation controls set to zero. The object of the tuning procedure is to produce a spectrum which varies by no more than 5 dB over the frequency region of interest. Since the equalizer can only attenuate bands of frequencies, the spectrum peaks are brought down to the level of the valleys. Additional gain is then applied to bring the spectrum back above the background noise level. When measurements are to be made at several locations in the room, a compromise

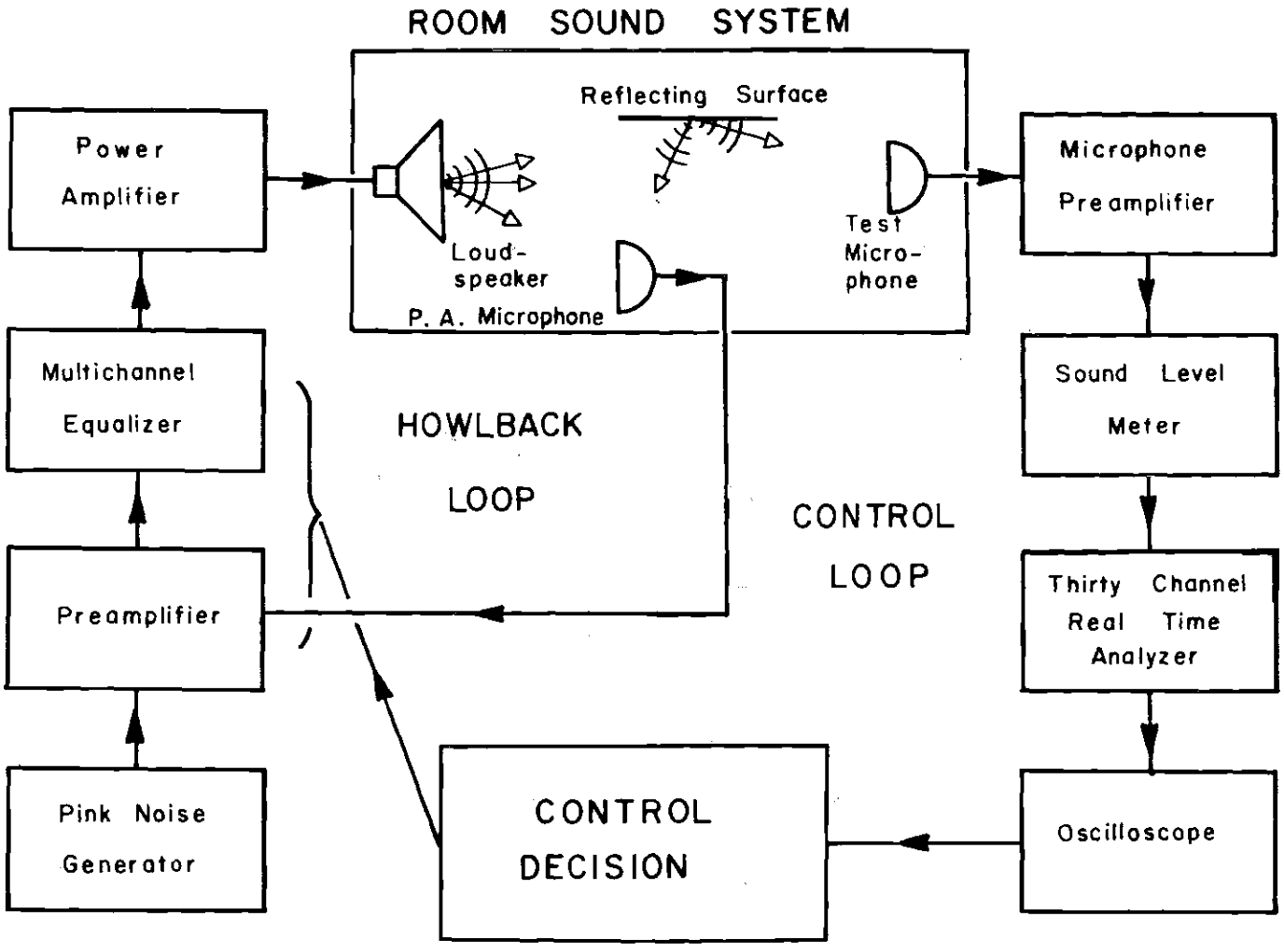

Figure 19. Signal Flow Diagram for Room Sound System Equalization.

between the equalizer settings must often be made. Extreme differences require directional loudspeakers with additional equalizers and amplifiers.

In public address systems, the introduction of a microphone changes the spectrum due to the reception of direct loudspeaker sound and reverberant sound. In cases of minor changes, the equalizer may be readjusted to correct for the interference effects. If adequate amplification can not be obtained without howlback at one or more frequencies, further equalization can be provided by decreasing the bandwidth of additional rejection filters and tuning them to the howlback frequencies.

CHAPTER V

RESULTS AND DISCUSSION

Filter Frequency Response

In Figure 20 the results of frequency response measurements on the worst case low and high frequency filters are shown. As indicated, the response is everywhere within 1 dB for the multiple feedback filter and 2 dB for the Wien Bridge filter. The reference input level was 20 dBm (7.75 Volts rms) and the noise levels were down by 75 dB for both filters.

Absolute Value Detector Response

The absolute value detector frequency response is shown in Figure 21 for three input levels: 0 dBm, -20 dBm and -30 dBm. Using the results from Table 2 for the linear full wave rectifier with sinusoidal input, the DC average output is $2/\pi$ times the sinusoid amplitude which in turn is given as $\sqrt{2}$ times the rms value which would be indicated on an input AC voltmeter. Thus a DC voltmeter reading either the detector or smoothing filter output would be $2/\pi\ \sqrt{2}$ times the rms input value. The vertical scale in the figure gives the additional loss of the detector output compared to the rms input where the ideal $(2/\pi)\ \sqrt{2}$ value is shown by the dotted line at -0.91 dB. By referring to equation (143), the drop in the curves as the signal level decreases is due to increased diode resistance at low current levels while the error caused for increasing frequency is due to reduced amplifier gain. The worst case error is

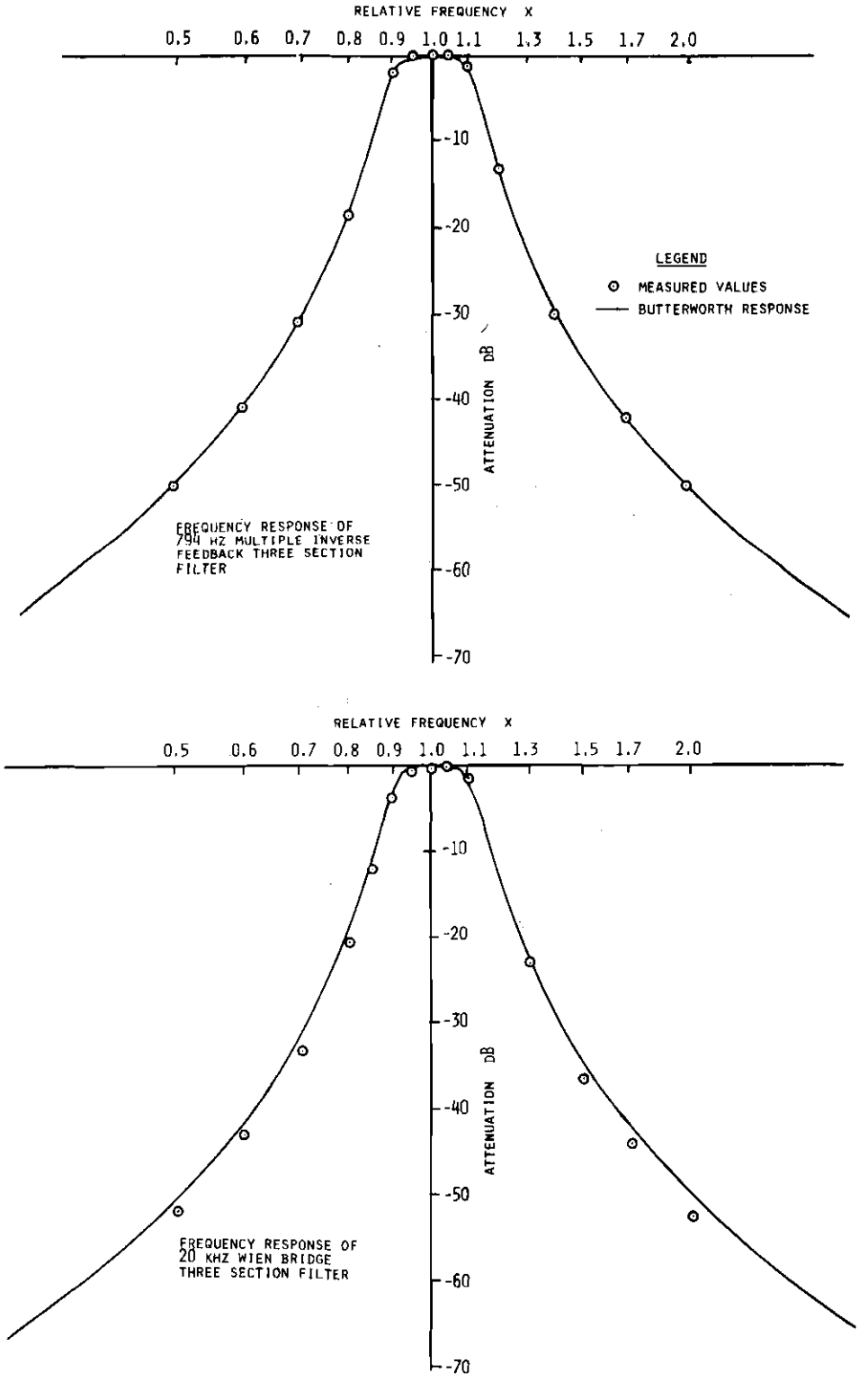

Figure 20. Highest Frequency Multiple Inverse Feedback and Wien Bridge Filters.

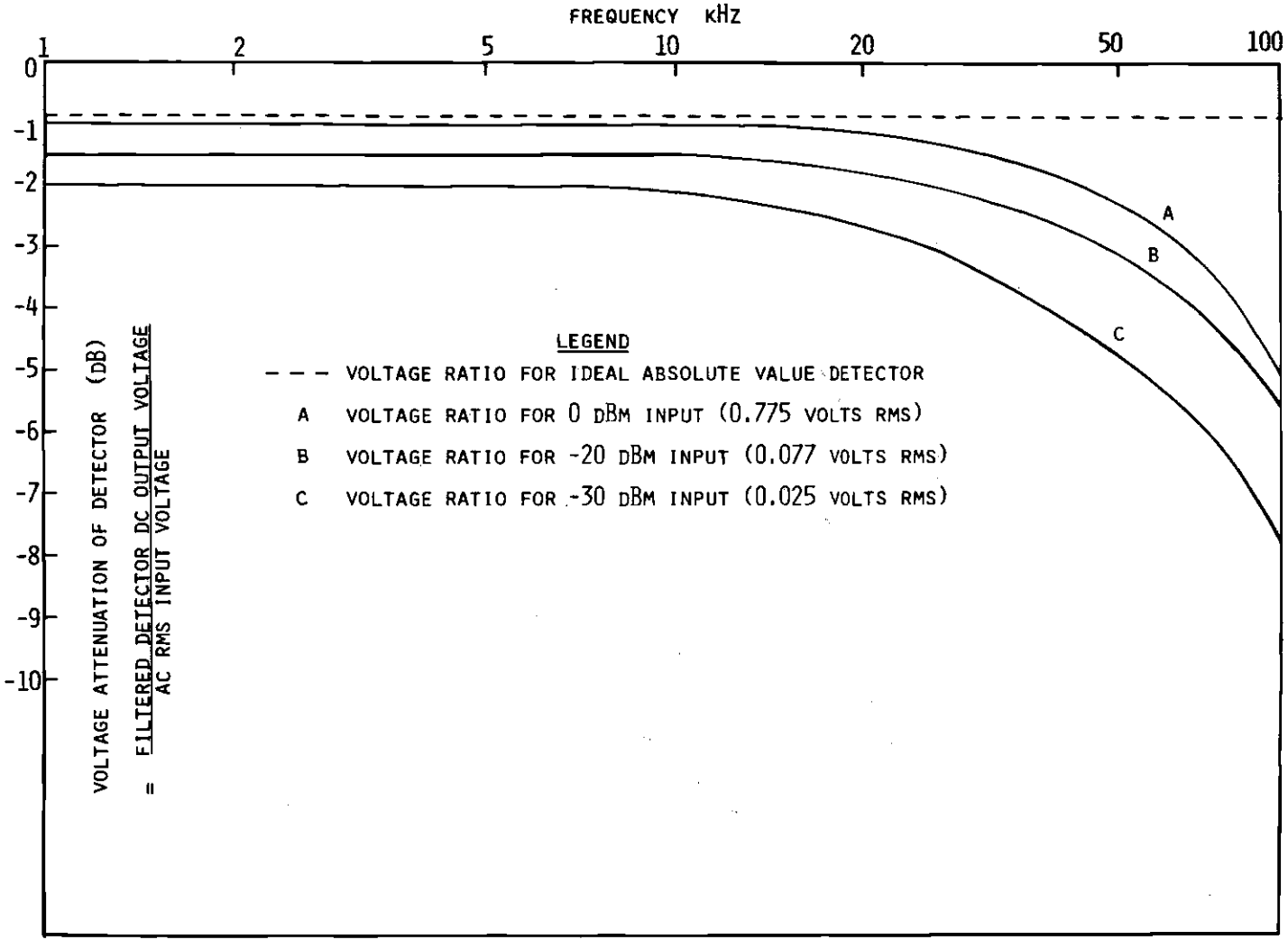

Figure 21. Absolute Value Detector Response for Three Input Sinusoid Levels.

1.6 dB which occurs at a frequency of 20 kHz with an input level of -30 dBm. For this reason, along with the existence of filter noise levels of -45 dBm, the input signal to the analyzer should be adjusted to give at least -20 dBm for all channels to be measured. Since the largest input signal possible without distortion is about 20 dBm, this allows a 40 dB display range with no more than 1 dB error at the highest frequency.

The Decibel Converter

The accuracy with which the decibel converter approximates a logarithmic response is best shown on the semilogarithmic scale in Figure 22. The deviation above 10 volts input is due to voltage drop losses on the finite base resistance in the transistor pair. The curve also deviates at inputs below 1 mV because of current loss due to the recombination loss of minority carriers at the transistor surface. For the usable detector output, the converter output is roughly -5 to +5 volts.

Detector Distortion Products

In the consideration of the low frequency fluctuations present in the outputs of the full wave and square law detectors, two approximations were made: (1) the bandpass filter was ideal and (2) in order to describe the power spectrum, only the convolution of the filtered spectrum with itself or $G_2(f)$ is needed. In the case of the square law detector, this last assumption was shown to be exact. Measurements were made on the two detectors using the apparatus shown in Figure 23A. The square law detector consisted of an Analog Devices 530 integrated

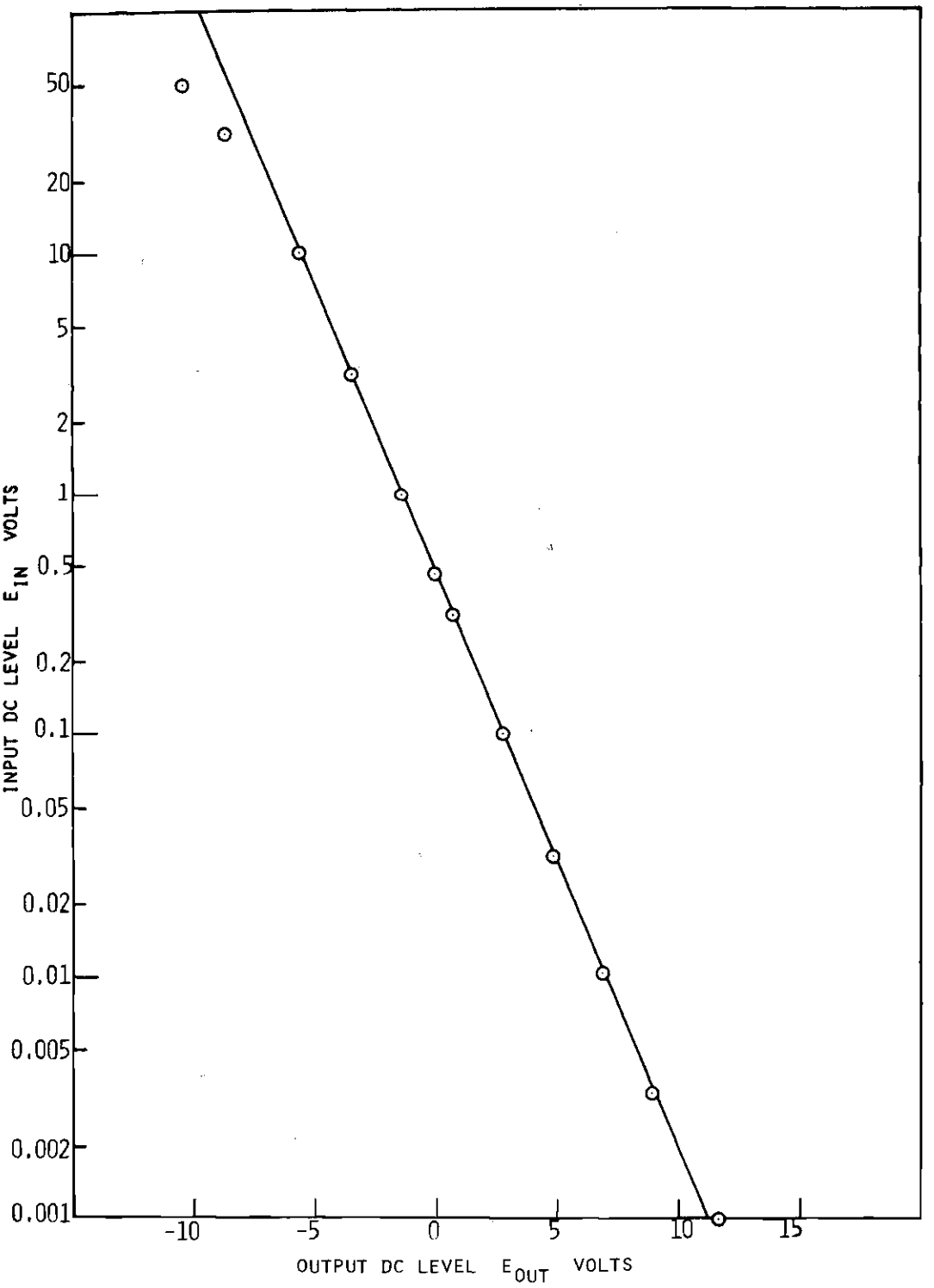

Figure 22. Output Voltage of Logarithmic Amplifier Versus Input Voltage.

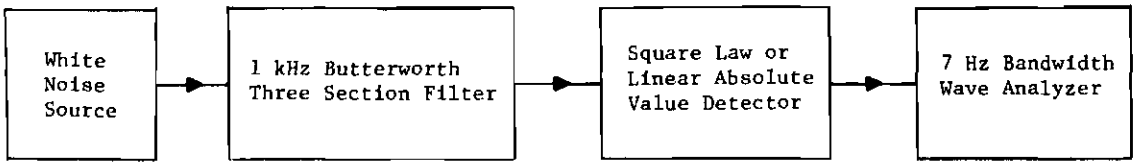

Figure 23A. Block Diagram of Apparatus Used for Measurement of Detector Distortion Products.

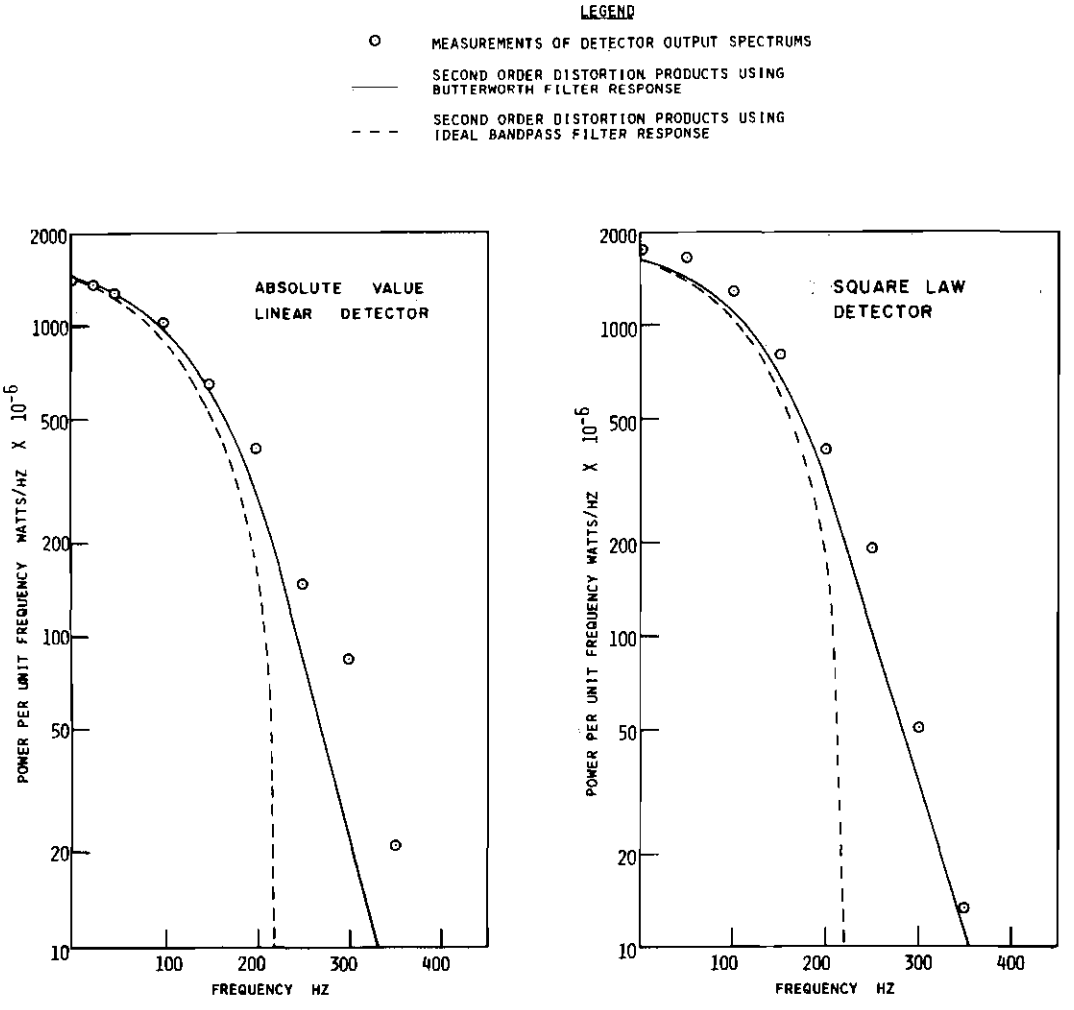

Figure 23B. Low Frequency Power Spectrums of Two Detectors with 1 kHz One Third Octave Noise Input of Bandwidth 221 Hz.

circuit multiplier with the two inputs tied together giving the output,

$$V_{Out} = (1/10 \text{ Volt})V_{In}^2 \quad . \tag{154}$$

The results for the 1 kHz bandpass filter with white noise input is shown in Figures 23B and 23C. The distortion products assuming an ideal bandpass filter is shown as a dotted line. The curve fits the measured values well for low frequencies but deviates for frequencies near the ideal filter band edge of 211 Hz since the filtered frequencies outside this bandwidth in the actual filter were neglected. When the convolution operation was numerically carried out for the Butterworth filter, the resulting dashed curves result. While this closely parallels the measurements for the square law case, the divergence at higher frequencies in the full wave detector results from neglecting the higher order distortion products.

Basic Noise Spectrums

Figure 24 shows photographs of the output spectrums obtained for three common noise sources: white, pink and USASI, the latter being noise which approximates the energy distribution of many kinds of speech and music [38]. The white noise spectrum is monotonically increasing with frequency due to the increasing bandwidth of the constant fraction one third octave bandwidth filters. This may be used to calibrate the vertical scale in decibels since for this noise the power is proportional to the filter bandwidth and doubles for every three filters. The resulting 3 dB increase indicates that each filter step and vertical mark on the scope face is equal to 1 dB .

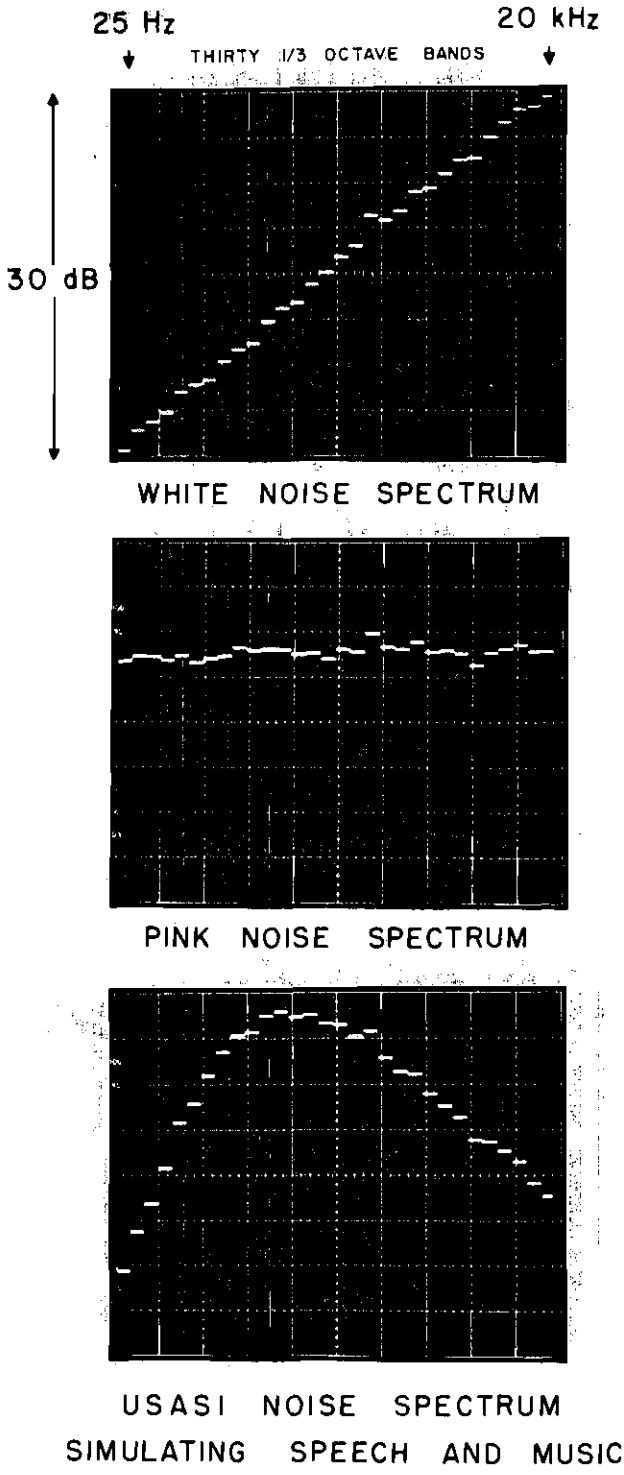

Figure 24. Output Spectrums for Three Common Noise Sources.

Pink noise, which is the most commonly used spectrum, has a flat response since the -3 dB/octave spectrum slope cancels the effect of increasing power with increasing bandwidth. Deviations from straightness due to the low frequency detector fluctuations appear to be less than 1 dB in this case.

The USASI spectrum is interesting because it shows the 6 dB/octave rolloff rate of the simple RC high pass and low pass filters which are used to modify the white noise spectrum. The two corner frequencies occur at 100 Hz and 320 Hz corresponding to the 7th and 12th filter bands. The spectrum does not appear to be symmetric because the filters are supplied with white noise instead of pink noise. As a result, the 3 dB/octave spectrum slope introduced by the increasing analyzer filter bandwidths goes uncompensated. The spectrum appears the same as for a pink noise driven system which has a 9 dB/octave rise rate and a 3 dB/octave fall rate. The increased sensitivity of the spectrum to rise rates agrees qualitatively with the limits of the spectral slopes of 15 and -21 dB/octave indicated by (30).

Room Equalization Measurements

The results of sound level measurements made in the laboratory are shown in Figure 25 where the room measurements and microphone locations are indicated. Since there was very little sound absorbent material in the room, the reflections from the walls, floor and ceiling caused deviations in the speaker and room pink noise response. The speakers consisted of a high frequency exponential horn mounted above a pair of 15 inch acoustic suspension woofers mounted in individual 2 foot square by 20 inch deep enclosures which were stacked vertically. In

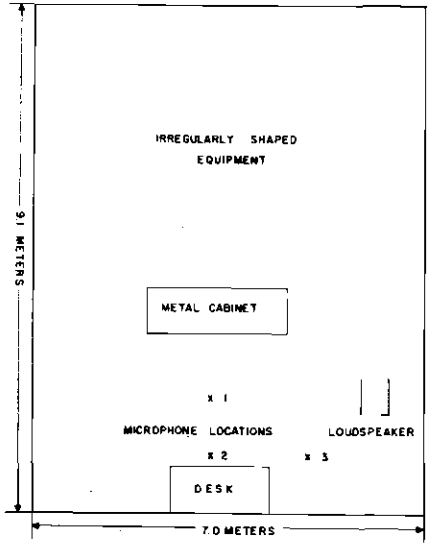

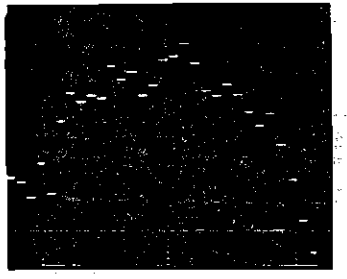

UNEQUALIZED ROOM SPECTRUM

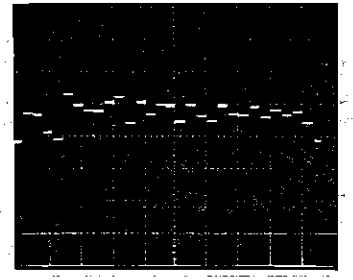

EQUALIZED SPECTRUM AT 1

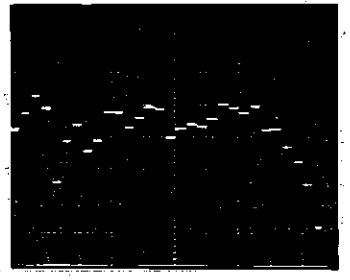

SPECTRUM AT 2

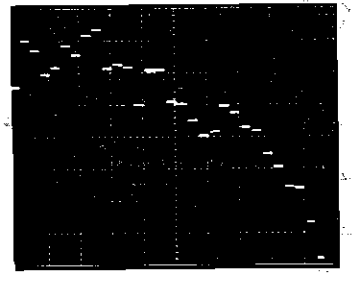

SPECTRUM AT 3 NEAR FLOOR

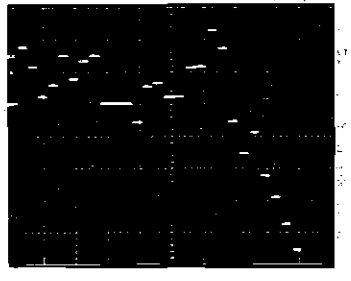

SPECTRUM AT 3 WITH HANDS
CUPPED AROUND MICROPHONE

Figure 25. Results of Sound Level Measurements Made in Laboratory.

the unequalized spectrum the response rolls off predictably at the rate of 12 dB/octave beginning at the frequencies 100 Hz and 8 kHz. The 8 dB dip at 63 Hz (5th filter) is due to destructive interference from the sound reflected from the front wall. Similar reflection from the floor and right side wall gives constructive interference for frequencies between 250 Hz and 316 Hz (filters number 11 and 12). The second peak at the octave from 800 Hz to 1.6 kHz corresponds to wavelengths of about 1 foot which are scattered from similar sized objects in the room. The room was then equalized at position 1 such that the spectrum deviates by no more than 2.5 dB from the average level. The microphone was next moved 42 inches off the speaker axis toward the right side wall. Except for increased intereference from this wall and increased rolloff past 8 kHz due to limited dispersion of high frequencies off the center axis of the horn, the spectrum remains essentially the same as at the previous position. The final two measurements were made at a third location which is 2 inches above the floor. Here the high frequency attenuation is increased since the microphone is even further from the horn center axis. The low frequency response is increased since the position is closer to the woofers and since the pressure due to low frequency standing waves is maximized near this boundary. The dip and peak near 1.6 kHz and 3.2 kHz correspond to sound waves reflected from the floor and combining destructively and constructively with the direct sound to the microphone. Since these frequency bands contain part of the intelligible portion of speech, this microphone location significantly changes the character of the sound. Such a position often occurs on the stage floor in a theater where the actors' voices are to be

recorded or reinforced. In the other spectrum measurement taken at this location, the observer's hands were cupped around the microphone as would be done to shield the microphone from unwanted sounds. The resulting column open at one end and closed at the other is approximately 3 inches long or one-half wavelength for frequencies near 2 kHz. The consequent reinforcement due to standing waves at the microphone gives the peak at filter number 20 and can cause howlback in public address systems for frequencies near this region of the spectrum.

CHAPTER VI

CONCLUSIONS

Two analyzers were constructed, one using single section filters and one using triple section filters. The triple section Butterworth filter provides adequate frequency resolution for one third octave bandwidth power spectrum measurements, since 88.3% of the total power falls within the nominal bandwidth for pink noise input. The single section filter transmits 65% of the total power within this band with the remainder flowing in from the adjacent octave bands. As a result, this instrument is used mostly as a tuning indicator for spectrums which are nearly flat as would be the case of an equalized room sound system driven by pink noise.

In the case of the three section filter accurate power measurements must take into account the finite attenuation of the filter skirts and the finite filter bandwidth. An optimum design bandwidth exists which adjusts the filtered power to that value which would be passed by an ideal filter with nominal fractional octave bandwidths. For nominal bandwidths other than one octave and for more than one filter section, the bandwidth correction is essentially the same for pink or white noise input. Consequently, the more easily calculated white noise bandwidth correction can be used to calculate the proper bandwidth for any n section filter with bandwidth on the order of an octave or less.

The independent frequency and gain controls of the multiple inverse feedback RC active filter facilitates the construction and tuning

of the three-section filter. With recently developed higher speed operational amplifiers, the inaccuracies accompanying the filter design at the higher frequencies can be reduced to 1.5% of the true filter response.

For a wide range of narrow band random noise inputs, the percent fluctuations around the D.C. output of the linear absolute value detector are nearly one half those of the square law detector. In rms measurements this means that the more easily constructed linear detector performs as well as the square law detector followed by a square root network. If the two detectors are calibrated to yield the same value for noise inputs, then a sinusoidal input to the absolute value detector will be 1 dB in excess of the true rms value of the square law circuit.

The absolute value detector may be synthesized with the 741 amplifier giving a frequency response error of less than 1 dB for signal levels over -30 dBm and for frequencies up to 20 kHz.

Room equalization measurements can be made with sufficient accuracy to identify destructive and constructive interference effects. A one third octave equalizer based on multiple inverse feedback filters may be used to adjust the spectrum response of a typical sound system to within ± 2.5 dB.

The RC smoothing circuit can be selected to give a worst case percentage fluctuation in the measured spectrum of 5% while at the same time it will respond to spectrum changes in under 20 sec.

APPENDIX A

DERIVATIONS

Output Correlation of Absolute Value Linear Detector with Random Noise Input

Assuming the detector output is given by equation (114), then using equations (113) and (114), the output correlation is

$$\psi(\tau) = \int_{-\infty}^{\infty} dV_1 \int_{-\infty}^{\infty} dV_2 \; \alpha^2 |V_1 V_2| \; \frac{1}{2\pi \, M^{\frac{1}{2}}} \; \exp \left[\frac{-(\psi_o V_1^2 + \psi_o V_2^2 - 2\psi_\tau V_1 V_2)}{2M} \right] \tag{A-1}$$

where

$$M = \psi_o^2 - \psi_\tau^2 \tag{A-2}$$

and

$$\phi_{\pm} = \psi_o V_1^2 + \psi_o V_2^2 \pm 2\psi_\tau V_1 V_2 \; . \tag{A-3}$$

This integral may be separated into a sum of four contributions where the polarity of V_1 and V_2 remain fixed. These integrals are simplified by substitution of voltage variables which are always positive and by then combining terms to give

$$\psi(\tau) = 2\int_{-\infty}^{\infty} dV_1 \int_{-\infty}^{\infty} dV_2 \; \alpha^2 \; V_1 V_2 \; \frac{1}{2\pi \, M^{\frac{1}{2}}} \; \exp \left(-\phi_- / 2M \right) +$$

$$2\int_{-\infty}^{\infty} dV_1 \int_{-\infty}^{\infty} dV_2 \; \alpha^2 \; V_1 V_2 \; \frac{M^{-\frac{1}{2}}}{2\pi} \; \exp \left(-\phi_+ / 2M \right) \; . \tag{A-4}$$

Rice [32] has evaluated integrals of this form for the half wave linear rectifier. The second integral differs from the first by the sign of the Φ term giving

$$\psi(\tau) = \frac{\alpha^2}{2\pi}\left[\left(\psi_o^2 - \psi_\tau^2\right)^{\frac{1}{2}} + \psi_\tau \cos^{-1}\left(-\psi_\tau/\psi_o\right)\right] +$$

$$\frac{\alpha^2}{2\pi}\left[\left(\psi_o^2 - \psi_\tau^2\right)^{\frac{1}{2}} - \psi_\tau \cos^{-1}\left(\psi_\tau/\psi_o\right)\right] . \qquad \text{(A-5)}$$

In this expression, the arc cosine is taken to have values between 0 and π. Equation (117) is obtained by introducing the normalized correlation variable ρ and then using the following identity based on the restricted definition of the arc cosine function

$$\cos^{-1}(-\rho) - \cos^{-1}(\rho) = 2\cos^{-1}(-\rho) - \pi . \qquad \text{(A-6)}$$

Output Correlation of the Square Law Detector with Random Noise Input

Assuming the detector output is given by equation (118), then using equations (114) and (115), the detector output correlation is

$$\psi(\tau) = \int_{-\infty}^{\infty} dV_1 \int_{-\infty}^{\infty} dV_2 \, \beta^2 V_1^2 V_2^2 \frac{M^{-\frac{1}{2}}}{2\pi} \exp\left(-\Phi_- / 2M\right) . \qquad \text{(A-7)}$$

The integrand can be separated into four terms involving fixed signs for the voltages V_1 and V_2. Substitution of positive voltage variables gives

$$\psi(\tau) = 2\int_{-\infty}^{\infty} dV_1 \int_{-\infty}^{\infty} dV_2 \; \beta^2 \; V_2^2 \; V_2^2 \; \frac{M^{-\frac{1}{2}}}{2\pi} \; \exp\left(-\Phi_- / 2M \right) +$$

$$2\int_{-\infty}^{\infty} dV_1 \int_{-\infty}^{\infty} dV_2 \; \beta^2 \; V_1^2 \; V_2^2 \; \frac{M^{-\frac{1}{2}}}{2\pi} \; \exp\left(-\Phi_+ / 2M \right) \quad . \qquad \text{(A-8)}$$

Integrals of this form have also been evaluated by Rice, giving

$$\psi(\tau) = \frac{\beta^2 \; \psi_o^2}{\pi} \left[\cos^{-1}(-\rho) \; (1 + 2\rho^2) + 3\rho \; (1 - \rho^2)^{\frac{1}{2}} \right] +$$

$$\frac{\beta^2 \; \psi_o^2}{\pi} \left[\cos^{-1}(\rho) \; (1 + 2\rho^2) - 3\rho \; (1 - \rho^2)^{\frac{1}{2}} \right] . \qquad \text{(A-9)}$$

Equation (119) results from the following identity based on the restricted definition of $\cos^{-1}\rho$

$$\cos^{-1}(-\rho) + \cos^{-1}(\rho) = \pi \quad . \qquad \text{(A-10)}$$

Power Series Expansion of Correlation of Absolute Value Linear Detector

The power series expansion of $(1 - \rho^2)^{\frac{1}{2}}$ is obtained from the binomial expansion

$$(1 - \rho^2)^{\frac{1}{2}} = 1 - \frac{\rho^2}{2} - \frac{\rho^4}{2 \cdot 4} - \ldots - \frac{(2n - 3)!!}{(2n)!!} \; \rho^{2n} - \ldots \qquad \text{(A-11)}$$

The series converges for $|\rho| < 1$.

The power series expansion for $\cos^{-1}(\rho)$ is obtained by integrating the power series expansion for $(1 - \rho^2)^{-\frac{1}{2}}$ giving

$$\cos^{-1}(\rho) = -\left(\rho + \frac{\rho^3}{2 \cdot 3} + \ldots + \frac{(2n-1)!!}{(2n)!!} \frac{\rho^{2n+1}}{(2n+1)} + \ldots \right) + C \, . \tag{A-12}$$

where the constant of integration C is found to be $\pi/2$ by evaluating the expression above at $\rho = 0$.

Expression (120) follows by substitution of these expressions into equation (117) and by combining coefficients of the powers of ρ.

Evaluation of the I_{2n} Integral

Using the results 3.821 - 12 and 3.836 - 2 in Gradshteyn and Ryzhik [24], the integral is

$$I_{2n} = \int_0^\infty \left(\frac{\sin x}{x} \right)^{2n} dx$$

$$= \frac{n}{(2n-1)!} \sum_{k=0}^{n-1} (-1)^k \binom{2n-1}{k} (n-k)^{2n-2} \, , \; n \geq 2 \, . \tag{A-13}$$

As n increases, the major contribution to the integral comes from the peak at the origin. A lower bound for this value is obtained by approximating the function sin x/x with the first two terms of its Taylor series expansion about x = 0. The integration is only carried out to the value $\sqrt{6}$ which is the value at which the value of this approximation reaches zero. The value is then approximated by

$$I_{2n} \approx \frac{1}{\pi} \int_0^{\sqrt{6}} \left(1 - \frac{x^2}{6}\right)^{2n} dx = \frac{\sqrt{6}}{\pi} \int_0^{\pi/2} \cos^{4n+1}\theta \, d\theta$$

$$= \frac{\sqrt{6}}{\pi} \frac{(4n)!!}{(4n+1)!!} \quad . \tag{A-14}$$

Summation of the First Ten Terms of $G_L(0)$

Applying the transform in equation (107) to the series approximation for the absolute value detector output correlation gives

$$G_L(0) = \frac{2}{\pi} \psi_o \alpha^2 \left[\delta(0) + \frac{1}{4B} \left(1 + \sum_{n=2}^{\infty} u_n\right)\right] \quad , \tag{A-15}$$

where

$$u_n = \left(\frac{(2n-3)!}{(n-2)!\, n!} \frac{1}{2^{2n-3}}\right)^2 2 I_{2n} \quad . \tag{A-16}$$

These values of u_n and I_{2n} are listed in Table 5.

Convergence of this series may be investigated by using the approximation (A-14) for large values of n, and by considering the ratio u_{n+1}/u_n. The ratio test gives an inconclusive result, but Raabe's Test shows that the series converges.

Table 5. List of Terms in Summation of $G_L(0)$

n	I_{2n}	u_n	Σu_n
1	0.500000	1.000000	1.000000
2	0.333333	0.041667	1.041667
3	0.275000	0.008594	1.050260
4	0.239683	0.002926	1.053186
5	0.215209	0.001287	1.054473
6	0.196963	0.000663	1.055136
7	0.182685	0.000379	1.055516
8	0.171120	0.000235	1.055750
9	0.161504	0.000154	1.055904
10	0.153349	0.000106	1.056010

Table 6. Circuit Values for Three Section Butterworth Filters and for Smoothing Filters

		CENTER FILTER				LOWER SHOULDER FILTER				UPPER SHOULDER FILTER				SMOOTHING FILTER	
n	F_o	R_1	R_2	R_5	C	R_1	R_2	R_5	C	R_1	R_2	R_5	C	R_t	C_t
1.	25.1	143	287	3.59	.2	63.0	254	.774	.5	52.0	210	.638	.5	180	64
2.	31.6	114	228	2.85	.2	50.0	202	.614	.5	41.3	167	.506	.5	150	64
3.	39.8	181	362	4.53	.1	39.8	161	.487	.5	32.8	133	.401	.5	100	64
4.	50.1	143	288	3.59	.1	79.0	320	.965	.2	65.2	265	.795	.2	86	64
5.	63.1	114	229	2.85	.1	62.7	255	.765	.2	51.8	211	.630	.2	86	64
6.	79.4	90.5	182	2.26	.1	49.8	203	.606	.2	41.1	168	.498	.2	86	64
7.	100	144	289	3.59	.05	79.1	323	.959	.1	65.3	268	.788	.1	51	64
8.	126	114	230	2.85	.05	62.9	258	.759	.1	51.9	214	.623	.1	47	64
9.	158	90.8	183	2.26	.05	49.9	206	.599	.1	41.2	171	.491	.1	47	64
10.	200	180	394	4.48	.02	39.7	165	.472	.1	32.8	138	.386	.1	39	64
11.	251	143	290	3.54	.02	63.0	265	.743	.05	52.0	221	.606	.05	39	64
12.	316	114	230	2.81	.02	50.1	213	.583	.05	41.3	179	.473	.05	39	64
13.	398	181	367	4.46	.01	39.8	172	.455	.05	32.8	145	.367	.05	27	64
14.	501	143	293	3.52	.01	79.0	345	.895	.02	65.2	297	.708	.02	22	64
15.	631	114	234	2.78	.01	62.7	281	.692	.02	51.8	246	.538	.02	22	64
16.	794	6.15	72.4	2.83	.05	6.48	79.7	3.24	.05	5.35	65.8	2.68	.05	18	64
17.	1.00K	4.88	57.5	2.25	.05	5.15	63.3	2.58	.05	4.25	52.3	2.13	.05	18	64
18.	1.26K	9.70	114	4.47	.02	4.09	50.3	2.05	.05	8.45	104	4.22	.02	18	64
19.	1.58K	7.70	90.8	3.55	.02	8.12	100	4.06	.02	6.71	82.5	3.36	.02	15	64
20.	2.00K	6.12	72.1	2.82	.02	6.45	79.3	3.23	.02	5.33	65.5	2.66	.02	15	64
21.	2.51K	4.86	57.3	2.24	.02	5.13	63.0	2.56	.02	8.46	104	4.23	.01	15	64
22.	3.16K	7.72	91.0	3.56	.01	8.14	100	4.07	.01	6.72	82.7	3.36	.01	18	32
23.	3.98K	6.13	72.3	2.83	.01	64.7	79.5	3.24	.01	5.34	65.7	2.67	.01	18	32
24.	5.01K	4.87	57.4	2.25	.01	5.14	63.2	2.57	.01	4.24	52.2	2.12	.01	18	32
25.	6.31K	7.74	91.2	3.57	.005	8.16	100	4.08	.005	6.74	82.7	3.37	.005	15	32
26.	7.94K	6.15	72.4	2.83	.005	6.48	79.7	3.24	.005	5.35	65.8	2.68	.005	15	32
27.	10.0K	4.88	57.5	2.25	.005	5.15	63.3	2.58	.005	42 5	52.3	2.13	.005	15	32
28.	12.6K	9.70	114	4.47	.002	4.09	50.3	2.05	.005	8.45	104	4.22	.002	10	32
29.	15.8K	7.70	90.8	3.55	.002	8.12	100	4.06	.002	6.71	82.5	3.36	.002	10	32
30.	20.0K	6.12	72.1	2.82	.002	6.45	79.3	3.23	.002	5.33	65.5	2.66	.002	10	32

$F_o = 10^{\frac{n+13}{10}}$ Hz

$f_o = F_o$
Q = 4.5188
A_o = 1.000

$f_o = F_o/\alpha$
Q = 9.079
A_o = 2.0091
α = 1.1005

$f_o = \alpha F_o$
Q = 9.079
A_o = 2.0091
α = 1.1005

APPENDIX B

DEFINITIONS

Autocorrelation

A measure of the similarity of a function with a displaced version of itself as a function of the displacement. The displacement is usually in terms of time and, when the displacement is zero, the value of the autocorrelation is equal to the mean square value of the function.

Octave

The interval between two sounds having a frequency ratio of two.

Sound Pressure Level

In dB, is 20 times the logarithm to the base 10 of the ratio of the pressure of the sound in a given band to the reference pressure. Reference pressures which are in common use are:

(a) 2×10^{-4} microbar ($20\ \mu N/m^2$)

(b) 1 microbar

Unless otherwise explicitly stated, it is to be assumed that the sound pressure is the effective (rms) sound pressure.

Transfer Function

Measure of the relation between the output signal and the input signal of a system, ordinarily the ratio of the respective Laplace transforms of the output and input signals.

BIBLIOGRAPHY

1. V. E. Freystedt, Zeits. f. techniche Physik 16, 533 (1935).

2. R. Roop and G. Cook, Report No. PB38054, Office of Technical Services, U. S. Department of Commerce (1942).

3. W. T. Kapuskar and C. J. Balmforth, Hewlett Packard Journal Vo. 20 No. 11 (1969).

4. W. R. Kundert, J. A. Lapointe, and G. R. Partridge, The General Radio Experimenter, Vol. 43 No. 5 (1969).

5. G. E. Valley and H. Wallman, in Vacuum Tube Amplifiers, p. 166, McGraw-Hill Book Co., New York, 1948.

6. L. W. Sepmeyer, J. Acoust. Soc. Am. 34, 1653 (1962).

7. L. W. Sepmeyer, J. Acoust. Soc. Am. 35, 404 (1963).

8. American Standard USAS S1.11 - 1966, p. 23 (1966).

9. A. E. Hastings, Proc. IRE 34, 126 (1946).

10. S. K. Mitra, IEEE Spectrum, p. 47, Jan. 1969.

11. W. R. Kundert, The General Radio Experimenter, Vol. 36 No. 10 (1962).

12. S. O. Rice, Bell System Tech. J. 23, 282 (1944); 24, 46 (1945).

13. C. T. Morrow, J. Acoust. Soc. Am. 30, 45 (1958); 30, 572 (1958).

14. H. Fletcher, Speech and Hearing in Communication, D. Van Nostrand, New York, 1953.

15. E. Zwicker, Acustica 10, 304 (1960).

16. M. R. Schroeder, J. Acoust. Soc. Am. 36, 1718 (1964).

17. C. P. Boner and C. R. Bonner, J. Acoust. Soc. Am. 37, 131 (1965).

18. R. V. Waterhouse, J. Acoust. Soc. Am. 37, 921 (1965).

19. A. B. Carlson, Communication Systems: An Introduction to Signals and Noise in Electrical Communication, p. 80, McGraw-Hill Book Co., New York, 1968.

20. American Standard USAS S1.11 - 1966, p. 22 (1966).

21. A. P. G. Peterson and E. E. Gross, Handbook of Noise Measurement 7th Edition, p. 95, General Radio Company, Concord, Massachusettes, 1972.

22. S. Butterworth, Wireless Engr. 7, 536 (1930).

23. H. Wallman, M. I. T. Radiation Lab. Rept. 524 (1944).

24. I. S. Gradshteyn and I. M. Ryzhik, Table of Integrals, Series and Products, Academic Press, New York, 1965.

25. L. W. Sepmeyer, J. Acoust. Soc. Am. 34, 1655 (1962).

26. A. G. J. Holt and J. K. Sewell, Proc. IEE 112, 2227 (1965).

27. R. C. Dobkin, Linear Brief LB-2, National Semiconductor Company, 1969.

28. J. G. Graeme, G. E. Tobey and L. P. Huelsman, Operational Amplifiers: Design and Applications, p. 315, McGraw-Hill Book Company, New York, 1971.

29. H. Nyquist, Bell System Tech J. 11, 126 (1932).

30. D. O. North, Paper read before I. R. E., Jan. 28, 1944.

31. A. B. Carlson, Communication Systems, p. 141.

32. S. O. Rice, Bell System Tech. J. 24, 158 (1945).

33. D. Middleton, J. Appl. Phys. 17, 778 (1946).

34. J. L. Lawson and G. E. Uhlenbeck, Threshold Signals, p. 63, McGraw-Hill Book Company, New York, 1950.

35. J. G. Graeme, G. E. Tobey and L. P. Huelsman, Operational Amplifiers, p. 245.

36. P. E. Gray et al., Physical Electronics and Circuit Models of Transistors, p. 42, SEEC Vol. 2, John Wiley and Sons, Inc., New York, 1964.

37. R. J. Widlar and J. N. Giles, Applications Bulletin APP - 124, Fairchild Semiconductor, Mountain View, California, 1966.

38. L. Accardi, Electronics, Vol. 43 No. 25, p. 75 (1970).

39. J. T. Kalb, EEE 19, 61 (1971).

40. S. O. Rice, Bell System Tech. J. 24, 67 (1945).

41. I. S. Gradshteyn and I. M. Ryzhik, p. 5.

VITA

Joel Thomas Kalb was born in Dublin, Georgia on July 22, 1946. He is the son of Henry T. and Martha Ann Kalb. He graduated from Coffee County High School, Manchester, Tennessee in 1964 and entered the Georgia Institute of Technology the same year. He received the degree of Bachelor of Science in Physics with highest honors in 1968. A Master of Science Degree in Physics was awarded in 1969.

He was the recipient of the Schlumberger Industrial Fellowship in 1971. During his several years in graduate school, he was a teaching assistant and also a research assistant in the School of Physics.